12

Technical Note

CEL

TN no. N-1515

title: LONG-TERM STRESS-STRAIN BEHAVIOR OF A SEAFLOOR SOIL

author: P. J. Valent

date: February 1978

sponsor: Office of Naval Research

program nos: 42-009

CIVIL ENGINEERING LABORATORY
NAVAL CONSTRUCTION BATTALION CENTER
Port Hueneme, California 93043

Unclassified
SECURITY CLASSIFICATION OF THIS PAGE (When Data Entered)

REPORT DOCUMENTATION PAGE

READ INSTRUCTIONS BEFORE COMPLETING FORM

1. REPORT NUMBER: TN-1515	2. GOVT ACCESSION NO: DN244145
3. RECIPIENT'S CATALOG NUMBER: CEL-TN-1515
4. TITLE (and Subtitle): LONG-TERM STRESS-STRAIN BEHAVIOR OF A SEAFLOOR SOIL	5. TYPE OF REPORT & PERIOD COVERED: Final; Jul 1974 - Jun 1975
	6. PERFORMING ORG. REPORT NUMBER
7. AUTHOR(s): P. J. Valent	8. CONTRACT OR GRANT NUMBER(s): RR031-01
9. PERFORMING ORGANIZATION NAME AND ADDRESS: CIVIL ENGINEERING LABORATORY, Naval Construction Battalion Center, Port Hueneme, California 93043	10. PROGRAM ELEMENT, PROJECT, TASK AREA & WORK UNIT NUMBERS: 61153N; RR031-01-01, 42-009
11. CONTROLLING OFFICE NAME AND ADDRESS: Office of Naval Research, Arlington, Virginia 22217	12. REPORT DATE: Feb 78
	13. NUMBER OF PAGES: 51
14. MONITORING AGENCY NAME & ADDRESS: Final rept. Jul 74-Jun 75	15. SECURITY CLASS. (of this report): Unclassified
	15a. DECLASSIFICATION DOWNGRADING SCHEDULE

16. DISTRIBUTION STATEMENT (of this Report)

Approved for public release; distribution unlimited.

17. DISTRIBUTION STATEMENT (of the abstract entered in Block 20, if different from Report)

18. SUPPLEMENTARY NOTES

19. KEY WORDS (Continue on reverse side if necessary and identify by block number)

Sediments, oozes, calcareous ooze, ocean bottom, soil mechanics, soil properties.

20. ABSTRACT (Continue on reverse side if necessary and identify by block number)

A calcareous deep-sea soil from the central Caribbean was subjected to a series of consolidation, triaxial shear, and triaxial shear creep tests to determine its response to loadings of engineering interest. The soil, classified as an inorganic silt, tended to densify during transport. Compression index C_c is 0.80; empirical terrestrial engineering correlations between C_c and other easily and rapidly measured index parameters may be in error by 30%. No significant crushing of the hollow foraminifera tests (shells) comprising the coarse-size fraction of the sediment was noted in the consolidation tests up to stresses of 1,530 kPa (32,000 psf).

continued

DD FORM 1 JAN 73 1473 EDITION OF 1 NOV 65 IS OBSOLETE

Unclassified
SECURITY CLASSIFICATION OF THIS PAGE (When Data Entered)

391 111

This coarse-sized fraction does, however, undergo significant crushing if material finer than 0.43 mm is removed, suggesting that the fine-sized fraction distributes loads on the coarse-sized test (shell) surfaces. Grain crushing may be partly responsible for the curved failure envelope developed from the triaxial shear tests. For specimens consolidated up to 30 kPa (4 psi) the angle of internal friction for the calcareous ooze is 0.60 rad (34 deg); specimens consolidated to greater pressures describe a flattening of the failure envelope to 0.49 rad (28 deg). Triaxial shear creep tests indicate that creep failure in this soil is not a significant engineering problem. The data suggest that material consolidated to higher stress levels than those used here (>100 kPa) and then shear loaded undrained will develop failure strains at stress levels less than 80% of short-term failure stress levels.

Library Card

Civil Engineering Laboratory
LONG-TERM STRESS-STRAIN BEHAVIOR OF A SEAFLOOR SOIL (Final), by P. J. Valent
TN-1515 51 pp illus Feb 1978 Unclassified

1. Seafloor soils 2. Soil loading I. 42-009

A calcareous deep-sea soil from the central Caribbean was subjected to a series of consolidation, triaxial shear, and triaxial shear creep tests to determine its response to loadings of engineering interest. The soil, classified as an inorganic silt, tended to densify during transport. Compression index C_c is 0.80; empirical terrestrial engineering correlations between C_c and other easily and rapidly measured index parameters may be in error by 30%. No significant crushing of the hollow foraminifera tests (shells) comprising the coarse-size fraction of the sediment was noted in the consolidation tests up to stresses of 1,530 kPa (32,000 psf). This coarse-sized fraction does, however, undergo significant crushing if material finer than 0.43 mm is removed, suggesting that the fine-sized fraction distributes loads on the coarse-sized test (shell) surfaces. Grain crushing may be partly responsible for the curved failure envelope developed from the triaxial shear tests. For specimens consolidated up to 30 kPa (4 psi) the angle of internal friction for the calcareous ooze is 0.60 rad (34 deg); specimens consolidated to greater pressures describe a flattening of the failure envelope to 0.49 rad (28 deg). Triaxial shear creep tests indicate that creep failure in this soil is not a significant engineering problem. The data suggest that material consolidated to higher stress levels than those used here (>100 kPa) and then shear loaded undrained will develop failure strains at stress levels less than 80% of short-term failure stress levels.

CONTENTS

INTRODUCTION

The consolidation and shear creep behavior of a calcareous deep-sea sediment was examined as a part of a study sponsored by the Office of Naval Research. The purpose of the study was also designed to evaluate the behavior with respect to observed sediment grain character changes. This soil behavior information is to be used in evaluating the long-term holding capacities of anchors embedded in these calcareous materials. Other work is underway at CEL evaluating the friction coefficients of calcareous materials against concrete and steel and evaluating the response of calcareous oozes to dynamic loading.

Calcareous oozes are seafloor sediments containing more than 30% calcium carbonate by weight (Sverdrup et al., 1942). Such oozes cover approximately 36% of the seafloor and are generally restricted to water depths less than 4,500 m (14,000 ft) (Noorany and Gizienski, 1970). The calcareous fraction of these sediments, which may be as large as 97% of the whole by weight (Holmes, 1965), is composed primarily of the skeletal remains of various planktonic animals and plants.

The most widely distributed sizes of foraminifera tests (shells) are 0.5 to 0.25 mm (Lisitzin, 1971), although tests of 1 mm diameter are common in the Caribbean samples of this study. The coarse-grained sediment fraction of predominantly whole tests is mixed in varying proportion with a finer-grained fraction composed of foraminifera test fragments; other marine life remains, such as those of the coccolithophoridae and the nannoplankton (dwarf plankton); inorganic-origin material, such as the clay minerals; and minor additional components (Sverdrup et al., 1942).

Most seafloor sediment examination has been confined to the measurement of bulk wet density, grain size distribution, specific gravity of the grains, Atterberg limits, carbonate content, organic carbon content, color, odor, and a strength index (e.g., Keller, 1967 and 1969; Hironaka and Smith, 1967; and Einsele, 1967). A few investigations have examined the primary consolidation* characteristics of calcareous oozes (Miller and Richards, 1969; Noorany, 1971; Bryant et al., 1973; and Terzaghi, 1940). Only one in-depth study of consolidation, including secondary compression, of a deep-sea sediment is known (Singh and Yang, 1971); that sediment was probably terrigeneous in origin and contained little calcareous material.

SAMPLE ACQUISITION AND INDEX PROPERTIES

Coring and Core Transport and Storage

Calcareous ooze samples were obtained from the USNS WILKES in the central Caribbean (Venezuelan Basin) at approximately latitude $15^{o}00'$ N. longitude $60^{o}20'$ W. A spade-box corer (Rosfelder and Marshall, 1967) with a sample box 0.20 x 0.30 x 0.46 m high was used to obtain two cores at each of two sites about 7.5 km apart in 3,930 m water depth. Details of the coring operation, of core storage and transport procedures, and of the sample changes during transport are reported in Valent, 1974. In summary, due to vibration in transit and due to partial drainage of the sediment pore water, the calcareous ooze samples densified and consolidated in transit, resulting in a bulk density change from 1.45 to 1.47 Mg/m^3 in one core and 1.46 to 1.47 Mg/m^3 in another.

---

*Primary consolidation is that component of soil compression governed by the hydrodynamic lag of soil pore fluid exiting the soil mass; secondary compression is a subsequent component governed by a relaxation of interparticle bonds and slight slippages, dislocations, and deformations of particles in the soil structure.

Index Properties

The measured soil classification properties are tabulated in Table 1. This calcareous ooze classifies as an inorganic silt (MH) in the Unified Soil Classification System (Anon., 1968). Valent (1974) provides more detailed sample description information. Difficulties in obtaining the grain size distribution and the Atterberg limits are detailed in the prior report; in summary, the hollow calcareous shells do cause testing and data interpretation difficulties.

ONE-DIMENSIONAL CONSOLIDATION CHARACTERISTICS

Volume Change Versus Pressure

Nine consolidation tests were started, two of which were stopped early: one due to a defroster malfunction in the refrigerator; the other due to a misalignment in the loading system. The specimen locations in the core boxes, their test conditions, and properties during the tests are given in Table 2. The void ratio versus logarithm of vertical effective stress curves e - $\log \bar{\sigma}_v$ for the tests on natural sediments are presented in Figure 1, and those for tests on "artificial" sediment are presented in Figure 2. Artificial sediment is composed of that portion of the natural sediment retained on the no. 325 sieve in a wet washing.

The water content and void ratio data have been corrected for salt content, assuming a salt concentration of 35 parts per thousand (after Richards, 1973). The void ratios herein are undoubtedly slightly in error because the specimens had undergone slight drying at the time of testing, causing the assumed salt content to be in error; the magnitude of the error is not significant in this study.

The e - $\log \bar{\sigma}_v$ curves of Figure 1 for the natural sediment specimens suggest a grouping of sorts based on the depth of the specimen in the

core box. Specimens C-1, C-2, and C-5 exhibit a tendency for a higher void ratio at any particular vertical stress $\bar{\sigma}_v$ than the remaining tests C-4, C-7, and C-8. The first three specimens listed came from the upper 50 mm (2 in.) of the core tubes, while the latter three came from 80 to 400 mm (3 to 16 in.) below the top of the tube. A slight soil difference with depth is the probable reason for this difference in behavior.

The e - log $\bar{\sigma}_v$ curves of Figure 1 start with quite different initial void ratios $\bar{e}_o$, maintain these initial different void ratios until reaching vertical pressures $\bar{\sigma}_v$ of about 10 kPa, and then start to converge. This behavior suggests the material being tested in each case is much the same, despite subseafloor differences in elevation. Differences in conditions imposed on the specimens during transport, storage, and handling are partly responsible for the large differences in specimen initial condition.

The e - log $\bar{\sigma}_v$ curve for the natural specimen tested under backpressure – C-1 – in the Anteus consolidometer shows no strong deviation from the other e - log $\bar{\sigma}_v$ curves developed without backpressure. This similar behavior suggests that for the calcareous ooze tested: (1) the growth of anoxic bacteria in the Anteus test specimen C-1, (2) the backpressuring of this particular soil, and (3) the maintained differences in test temperature probably do not have a significant influence on consolidation of the calcareous ooze tested. (Note: It is also possible, though much less likely, that anaerobic growth, backpressuring, and temperature difference may have compensating effects on the e - log $\bar{\sigma}_v$ function, resulting in no net difference in consolidation response.)

Figure 1 indicates that the e - log $\bar{\sigma}_v$ curve for the calcareous ooze tested does not become a straight line at higher pressures as is usually the case (Taylor, 1948). Possible causes for this condition are twofold: (1) this particular material may simply be more compressible at higher pressures than are those that soils engineers are accustomed to working with, and (2) the continued increase in slope may possibly be due to the extrusion of material past the porous stone at higher pressures (Altschaeffl, 1973).

Roberts (1964) found increasing compressibilities in quartz sands at one-dimensional (1-D) compression pressures of 140 MPa (20,000 psi). The increased compressibilities were directly linked to quartz grain crushing at these high pressures. It is the author's contention that grain breakdown of sorts is also responsible for the increasing compressibility of the subject calcareous ooze at loads of engineering interest. Attempts to support this hypothesis by verifying that grain crushing had taken place during 1-D consolidation of natural specimens were unsuccessful. Possibly the dominant compression mechanism in a graded soil sample is not crushing of the hollow shells; but, rather, very high nonrecoverable deformations of the shells without physical breaking or puncturing. No significant change in the grain size distribution was noted, nor was a significant increase in the proportion of "punctured" shells noted.* Subsequently, 1-D consolidation tests were conducted on artificial specimens composed of only that material retained on the 325 sieve – material in these tests did undergo grain crushing and puncturing. Tests of such an artificial specimen, however, do not verify that grain crushing has occurred in the natural specimen.

The second possible reason for the apparent increase of compressibility with consolidation pressure is extrusion of material past the porous stone at higher pressures. Some support of this idea is given by consolidation tests C-4 and C-8 (Figure 1), conducted with a load increment ratio $\Delta\bar{\sigma}/\bar{\sigma}_v$ of 2. All those e - log $\bar{\sigma}_v$ curves developed using a load increment ratio of 1 indicate continuing increasing slope of the curves with increasing log $\bar{\sigma}_v$ (C-1, C-2, C-5 and C-7 of Figure 1). Both those e - log $\bar{\sigma}_v$ curves developed using a load increment ratio of 2 show markedly different behavior (C-4 and C-8 of Figure 1), describing essentially straight line curves from pressures of 200 kPa to 1,500 kPa. Consolidation test C-4 is of note because considerable squeezing was first noted during a test with this specimen. Approximately 2.5% of the

*Punctured shells are ones that are at least 80% intact.

specimen solids were extruded between the stone and consolidometer ring with most of this extrusion noted as occurring at the outset of the load increment from 195 kPa to 589 kPa. Thus, specimen C-4 describes an essentially straight line e - log $\overline{\sigma}_v$ curve, while exhibiting considerable squeezing. This behavior seems to contradict the hypothesis that extrusion is responsible for downward curved e - log $\overline{\sigma}_v$ curves; in reality, it does not. Extrusion in Test C-4 occurred selectively during the load increment from 195 kPa to 589 kPa, and extrusion was noted as significantly less in subsequent load increments. The extrusion in test C-4 may have occurred earlier than in the other consolidation tests, depressing the e - log $\overline{\sigma}_v$ curve earlier and, in effect, straightening that curve. Thus, soil extrusion is noted as a factor in straightening e - log $\overline{\sigma}_v$ curves (with $\Delta\overline{\sigma}_v/\overline{\sigma}_v = 2$) that might otherwise have been curved downward. The use of smaller load increment ratios, such as the $\Delta\overline{\sigma}_v/\overline{\sigma}_v = 1$ of tests C-1, C-2, C-5 and C-7, may very well retard and delay such extrusion to pressures greater than 589 kPa. Such a mechanism, if it does occur, would help support Altschaeffl's hypothesis that squeezing is responsible for the errant e - log $\overline{\sigma}_v$ curve data.

Volume change versus pressure data by convention are quantified in terms of the slopes of straight line approximations to the e - log $\overline{\sigma}_v$ curve. The slope of the straight line approximation to the latter part of the curve during loading is called the compression index C_c. The values of C_c obtained in the tests on the undisturbed sediment ranged from 0.64 to 0.89 with an average and median of 0.75 (Table 3).

Various empirical relationships have been used to predict the C_c for cohesive soils. Some of these relationships and the resulting empirical predictions of compression index are listed in Table 3. Those predictive relationships using the Atterberg liquid limit yield values of compression index which are too low, yet those which use the initial void ratio e_o and the natural water content w yield values which are too high. These differences suggest that calcareous oozes are somewhat different in their compression behavior from terrestrial soils and that standing empirical relationships for the prediction of compression behavior do not apply.

Reasons for the deviations in magnitude between experimentally measured and empirically predicted C_c values probably lie in the character of the soil grains. First, those relationships that predict C_c based on the Atterberg liquid limit w_L may yield C_c values that are too low because of the silty nature of the ooze and because of the relatively low affinity of the carbonate particle surface for adhered water. The most significant factor causing the relatively low w_L value has not been established. Those relationships that predict C_c based on initial void ratio e_o or water content w yield C_c values that are too high because the calcareous ooze contains much of its void space and water within hollow animal shells (primarily those of foraminifera). The void space and pore water within the shells of the natural specimens do not substantially enter into the soil compressibility at the loadings attained (see next section).

Grain Crushing in Artificial Specimens

Grain size distribution tests made on specimen C-2 after loading to 1,530 kPa and on an undisturbed specimen indicated no significant change in the grain size distribution as a result of 1-D compression. Visual examination revealed holes existing in the walls of many shells before and after consolidation testing, making an assessment as to the effect of compression testing difficult. A possible explanation for the apparent negligible influence of the 1,530 kPa vertical compressive stress on the fragile animal shells is that the fine-grained fraction of the ooze material acts as a load distributor, evenly stressing the shells much like the loading received by a flexible pipe beneath an earth fill. To test this hypothesis, artificial specimens C-3 and -9, composed of ooze material retained on the no. 325 sieve, were subjected to the same conditions as the natural specimens. The e - log $\bar{\sigma}_v$ curves for these two specimens have been presented in Figure 2.

Specimen C-3 exhibited very little compression during the early stages of the consolidation test followed by an abrupt steepening of the

e - log $\bar{\sigma}_v$ curve. The start of the very steep curve is believed to mark the start of significant grain crushing; i.e., between 50 and 200 kPa (about 1,000 and 4,000 psf). The results of grain size analyses on the 1-D compression specimen C-3 after testing and on the excess sample (which is considered representative of the specimen's initial state) are presented in Figure 3. The grain size curves do confirm that shell crushing did occur in the artificial specimen during compression. Most crushing occurred in the medium sand size fraction, with 30% of the material reduced to a size passing the no. 325 sieve. The fact that significant crushing was noted in the specimen made up without fines, while no significant crushing was noted in the natural specimen with fines, serves to confirm the role of the fine-grained fraction in the protection of the foraminifera shells against crushing in this particular calcareous ooze sample.

Figure 4 illustrates the nature of that portion of the sediment retained on the no. 30 sieve before 1-D compression. Note that some of the shells have already been broken, very likely during ingestion by planktonic or bottom-dwelling organisms or from partial dissolution or possibly during coring, disaggregation, and sieving of the specimen. Figure 5 illustrates the changes that took place in that grain size fraction during the loading of compression specimen C-3. Before compression loading, Figure 4 shows 9% of the plain spherical shells to be partially broken; after compression loading, Figure 5 shows 38% of the plain spherical shells to be partially broken.

It is significant to compare the behavior of the artificial calcareous ooze specimen with that of a typical mineral sand (grains of quartz). Similar 1-D consolidation tests on quartz sand indicate the initiation of grain crushing at 14,000 to 21,000 kPa (2,000 to 3,000 psi) (Lambe and Whitman, 1969) versus crushing initiation at 50 to 200 kPa for the calcareous shell grains.

Time Rate of Secondary Compression

After the conclusion of primary consolidation (i.e., marked presumably by the dissipation of all excess pore pressure) the height change of the natural specimen as a function of time is described quantitatively by the secondary compression index C_α,

$$C_\alpha = \frac{\Delta H}{H \times \Delta \log_{10} t} \qquad \text{(Lambe \& Whitman, 1969)}$$

where

$\frac{\Delta H}{\Delta \log_{10} t}$ = slope of the secondary consolidation portion of the height change versus log time curve

H = specimen height at the start of that load increment.

Measured values of C_α are presented in Figure 6.

Figure 6 shows quite clearly that there is a marked increase in the magnitude of C_α with increase in the consolidation pressure across the entire consolidation pressure range. Mesri (1973) states that for most clays C_α will usually increase with increasing $\bar{\sigma}_v$ until reaching the preconsolidation pressure, after which C_α will usually decrease with increasing $\bar{\sigma}_v$. The calcareous ooze behavior (i.e., C_α versus $\bar{\sigma}_v$) does not agree with the latter portion of Mesri's statement; that is, these calcareous ooze data show that, for consolidation pressures well in excess of the maximum past pressure, the C_α value continues to increase with increase in $\bar{\sigma}_v$.

Figure 6 suggests that C_α for those specimens tested at room temperature does not differ significantly from C_α for those tested under refrigeration. Mesri (1973) reports similar findings for an inorganic clay.

The literature mentions the possible influence of temperature change on the C_α value by virtue of the expansion or contraction of the consolidometer ring (Mesri, 1973). The room temperature of the laboratory varied from about 24C (75F) to about 29C (85F) in one cycle during a 24-hr period. Undoubtedly, the specimen and its confining ring experienced this same cyclic variation. During testing of specimens C-2 and C-4 in the refrigerator, temperatures were noted as varying from about 3C (38F) to about 10C (50F) – the same magnitude of temperature range. However, this temperature cycle occurred about once every 20 min – rather than once per day. The consolidometer ring and specimen probably did not have time to experience a temperature range anywhere near that measured in the room. The variation did occur, however, about 100 times per 24-hr period. Note again that the C_α values from both room temperature and refrigerated specimens during testing are essentially the same, suggesting that the temperature variation and cycling did not have a significant effect on C_α values.

One load increment was maintained on specimen C-5 to examine the specimen response to load over a duration of some 15 days. This test revealed a direct response between temperature and displacement dial reading – temperatures of 8C (47F) yield dial gage displacement readings about 0.0002 in. greater than temperatures of 6C (42F) (Figure 7). This variation could possibly be due entirely to the differential expansion-contraction in the displacement measuring system. In addition, however, if we assume that the brass consolidometer ring does experience the temperature difference of 2C (5F), and if the confined specimen is assumed to maintain constant volume during the change in diameter of the ring, then the specimen should change height by 0.0001 in. – consistent with the measured displacement. Quite possibly, then, the specimen was being cyclically deformed as a result of the measured temperature variations.

Figure 8 is a replot of the data presented in Figure 6, but this time the effect of load increment ratio $\Delta\bar{\sigma}_v/\bar{\sigma}_v$ is sought. The data obtained suggest no significant trend with $\Delta\bar{\sigma}_v/\bar{\sigma}_v$, although, for low values of the vertical effective stress, the higher load increment ratio $\Delta\bar{\sigma}_v/\bar{\sigma}_v = 2$ seems to have a tendency to produce slightly higher values of

C_α. Mesri (1973) notes that most researchers have found that load increment ratio has no significant influence on C_α, as is found with this calcareous ooze.

The magnitudes of the secondary compressions experienced with the calcareous ooze specimens were actually quite small – $C_\alpha < 0.007$ except for one spurious value of 0.010. Lambe and Whitman (1969) list such magnitudes for C_α as belonging to the less plastic normally consolidated clays (C_α = 0.005 to 0.020) or to slightly overconsolidated clays. Mesri (1973) discusses secondary compression magnitudes in terms of the coefficient of secondary compression $\varepsilon_{\alpha p}$ where:

$$\varepsilon_{\alpha p} = C_\alpha/(1 + e_p)$$

where e_p = the void ratio at the beginning of the linear portion of the e - log t curve. The indices C_α, obtained herein, converted into the coefficient $\varepsilon_{\alpha p}$ have values between 0.014 and 0.31 percent. Mesri states that secondary effects probably would not be of any practical consequence in soils with $\varepsilon_{\alpha p}$ less than 0.1%. It would appear, therefore, that secondary compressions in calcareous oozes of the type tested will not be of engineering significance.

STRENGTH CHARACTERISTICS

Four natural specimens and one artificially prepared specimen were consolidated isotropically and sheared undrained; i.e., CIU tests. Characteristics of the specimens are reported in Table 4 and principal stress difference $\bar{\sigma}_1 - \bar{\sigma}_3$ versus axial strain ε results are presented in Figure 9. Those specimens consolidated under isotropic stress of 37.9 kPa (5.49 psi) and less (i.e., specimens T-1, T-2, and T-4), reached 65% to 70% of peak strength after relatively little straining – 1% or less. With further straining, the principal stress difference increases gradually reaching a peak value at between 16% to 20% strain. From this point, the principal stress difference appears to remain near constant. These

specimens bulged uniformly during the continued axial strain, and no shear failure plane could be identified. Specimen T-4, consolidated to 109.8 kPa (15.94 psi), reacted much more rapidly with the principal stress difference reaching 84% of the peak difference at 1% axial strain and with the principal stress difference actually peaking at 7% strain. With continued strain, the principal stress difference then decreases, reaching a 15% reduction at 20% axial strain. This specimen exhibited a well-defined failure plane.

The significance of this stress-strain data is best understood after replotting the stress data as stress path information as in Figure 10. Here the quantity $(\bar{\sigma}_1 - \bar{\sigma}_3)/2$ was plotted versus $(\bar{\sigma}_1 + \bar{\sigma}_3)/2$ for the duration of each shear test to produce so-called stress paths for each test. The quantity $(\bar{\sigma}_1 - \bar{\sigma}_3)/2$ is a function of the shear stress on a plane within the specimen; and the quantity $(\bar{\sigma}_1 + \bar{\sigma}_3)/2$ is a function of the normal stress on that plane (Lambe and Whitman, 1969). The stress paths of Figure 10 are indicative of the stress history of the calcareous ooze material (Lambe and Whitman, 1969). They indicate that specimen T-2, consolidated to 6.5 kPa (0.94 psi), was overconsolidated in terms of behavior, when sheared; specimen T-3, consolidated to 109.8 kPa (15.93 psi), was normally consolidated; and specimen T-1, consolidated to 37.9 kPa (5.49 psi), was lightly overconsolidated. A soil element is defined as being normally consolidated if it is now in equilibrium under the maximum stress it has ever experienced, and as being overconsolidated if it is at equilibrium under a stress less than that to which it was once consolidated (Lambe and Whitman, 1969). The overconsolidated behavior of specimen T-2, that consolidated to 6.5 kPa, need not necessarily be indicative of soil condition on the seafloor but is likely the result of sample state change during coring, transit, storage, and specimen test setup.

Figure 10 also presents the stress difference-strain data from CIU test T-10. Specimen T-10 was artificially reconstituted from that portion of the calcareous ooze material retained on the no. 325 sieve as described earlier. The specimen was formed by spooning the fine sand material into the specimen mold and then lightly tapping the mold to

somewhat densify the material. The resulting specimen would probably classify as loose. The stress-strain behavior of specimen T-10 differed considerably from that of the natural soil specimens. The stress-strain curve developed a pronounced break in slope at a principal stress difference of about 28 kPa, about 33% of the peak principal stress difference. The stress path plot of artificial specimen T-10 is helpful in evaluating specimen behavior. Interpretation of the stress path plot shows that the specimen excess pore pressure, Δu, increases during the early shear loading of the specimen reaching a ratio of excess pore pressure to consolidation pressure $\Delta u/\sigma_c$ of 0.58. This rise in pore pressure is probably due to grain reorientation into a more dense arrangement; grain crushing is not thought to be a strong contributor at this low axial stress. When the principal stress difference reaches about 33% (i.e., 30 kPa) of the peak principal stress difference, then the specimen first starts to shear, as indicated by the decrease in Δu. A likely hypothesis for this behavior is that soil grains are being forced to ride up and over each other, an action accompanied by a tendency toward specimen expansion largely countered by the decrease in excess pore fluid pressure. This grain rearrangement and reorientation continues, with the stresses on the soil grains gradually building until the peak principal stress difference is reached at about 12% axial strain. After this peak, a shear plane starts to develop, accompanied by a reversal in the direction of pore pressure change (to increasing Δu). This shear plane was clearly evident after 14.6% axial strain. The increasing excess pore pressure is related to a volume decrease in the specimen somewhere, and the most obvious place is in the shear zone. The stress path of T-10 in Figure 10 shows a complete reversal of stress-path direction upon reaching the peak principal stress difference, and traces a route directly on the established strength envelope for the natural calcareous ooze. In other words, the effective angle of internal friction of the natural soil at these stress levels – $\overline{\phi}$ = 0.60 rad (34.5 deg) – applies also to the artificial specimen T-10 with those fines passing the no. 325 sieve removed.

At the completion of drained shear tests T-5 and T-6, the strength envelope had been reasonably well-defined and confirmed over the region of interest. However, the crushing of calcareous ooze shells had not been detected in any specimen's behavioral response to triaxial shear loading. It was decided to utilize the available triaxial equipment to maximum-rated capacity to determine the influence of grain crushing on the effective strength envelope and on the angle of internal friction. Specimens T-7 and T-8 were consolidated to the maximum confining pressure possible and then sheared drained. Triaxial test T-7 experienced some aberrations in the stress-strain relationship suggestive of binding of the loading ram; (i.e., steps in the stress-strain curve of Figure 11). Specimen T-8 was then tested identically to specimen T-7, and did verify the former data.

Specimen T-9 was then consolidated to a stress selected so as to provide an intermediate data point with respect to those available for determining the soil failure envelope and the angle of internal friction. Specimens T-7, T-8, and T-9 served to delineate a slightly different soil failure envelope at higher pressures with a lower angle of internal friction $\overline{\phi}$ = 0.49 rad (28.2 deg) – versus $\overline{\phi}$ = 0.60 rad (34.5 deg) as determined from those tests at lower effective stresses (see Figure 10).

A decrease in the effective angle of internal friction with increasing stress level has been observed by others in materials which were undergoing grain crushing at the higher stress levels (e.g., Marsal, 1967; Carrier et al., 1973). It is quite likely that this grain crushing phenomenon is responsible for the decrease in slope of the soil strength envelope from 0.60 to 0.49 rad. A second reason* for the slope change: some small excess pore pressure may have existed within the specimens during shear and especially at failure. Such an excess pore pressure would cause the real effective confining stress to be less than the calculated $\overline{\sigma}_3$ and would result in a realized principal stress difference $\overline{\sigma}_1 - \overline{\sigma}_3$ that would be slightly smaller than it should really be. The slight difference in the maximum principal stress differences measured in CID shear tests

*Not highly regarded by the author.

T-5 and T-6 (Figure 10) may be a manifestation of this incomplete drainage, if that condition did indeed exist. Shear test T-5 with the slightly higher maximum principal stress difference took 180 hr to reach 13% axial strain, while T-6 took 6 hr. However, the difference in behavior between T-5 and T-6 can be just as easily attributed to possible differences in the specimen composition or to possible differences in equipment performance.

If, however, the difference in specimen behavior noted above is largely due to a slight excess pore pressure not dissipated during the 8-hr CID triaxial shear tests, then the maximum principal stress difference data from CID tests T-7, T-8, and T-9 are also likely in error on the low side. Such an error would lower the resulting plotted line of maximum principal stress difference and, thus, could be responsible for the lower angle of internal friction described in tests T-7, T-8, and T-9. An interesting question is whether or not the very close agreement of data from triaxial tests T-7 and T-8 tends to disprove the excess pore pressure explanation for the low angle of internal friction. The data from these two tests are virtually identical, even though the specimens come from different box cores taken 7.5 km apart. It is difficult to believe that the pore pressure response to the shear loading for these two specimens would be identical, unless it had already virtually reached zero – i.e., the excess pore pressure induced by shear had essentially dissipated. Please note that tests T-7 and T-8 were alike even with respect to the time required to reach maximum principal stress difference – about 6 hr in each case.

CREEP CHARACTERISTICS

Drained Creep

Table 5 summarizes information on the 16 creep specimens. Figure 12 presents the axial strain versus log time results of the series of

seven drained triaxial shear creep tests, all consolidated to about 38 kPa, then incrementally loaded according to the same loading plan with loading stopping at different percentages of the drained triaxial shear strength corresponding to that $\bar{\sigma}_c$. This $\bar{\sigma}_c$ = 38 kPa was selected because it corresponds to the vertical effective stress at a soil depth of 10 m, that depth at which direct embedment anchor flukes can be expected to be functioning in this soil. Note that time zero on the log scale of Figure 12 is the time of application of the last increment of shear load.

This set of creep curves show that, for the drained mode of shear, creep in this calcareous ooze is not a problem at the consolidation pressure used. At this consolidation pressure $\bar{\sigma}_c$ of 38 kPa, the log rates of strain are all decreasing, even for that specimen loaded to 80% of failure, indicating that creep shear failure in the drained state is not of engineering significance.

Singh and Mitchell (1968) presented a simple three parameter phenomenological equation to describe the strain rate-time and strain-time response of cohesive soils:

$$\varepsilon - a = \frac{A}{1-m} \times 10^{\alpha \bar{D}} \times t^{1-m}$$

where

ε = strain

a = constant of integration

A = fictitious strain at zero deviator stress

$\bar{D} = \frac{(\bar{\sigma}_1 - \bar{\sigma}_3)_{creep}}{(\bar{\sigma}_1 - \bar{\sigma}_3)_{failure}} \times 100$ = ratio of the principal stress difference applied to the principal stress difference at shear failure, %

m = straight line slope of logarithm strain rate versus logarithm time curve

α = slope of the midrange linear portion of the logarithm strain rate versus principal stress difference curve

t = time

This form of relationship is reported applicable to terresterial clays under a wide range of conditions (i.e. clays undisturbed or remolded, wet or dry, normally consolidated or overconsolidated, or tested drained or undrained). This relationship is reported valid over a range of creep stress intensities from about 30% to an upper limit, possibly as high as 90%, of the initial soil strength. The upper limit depends on the susceptibility of the soil to fail in creep rupture. The suitability of this relationship for describing the drained creep behavior of this calcareous ooze was examined with reasonably favorable results.

Constants for the phenomenological relationship were developed graphically. First, strain rates at various values of time were computed graphically. These strain rates were then plotted against time on log-log plots (Figure 13). Singh and Mitchell (1968) present data indicating that the creep strain rate versus time data of a series of tests on similar test specimens do describe a series of parallel lines. For the calcareous ooze examined, the $\dot{\varepsilon}$ versus log t data do exhibit a distinct linear tendency for those specimens loaded to 55% of failure and greater, yielding an average slope m of 1.08. Specimens loaded to 34% of failure and less digressed considerably from this straight line pattern.

The constant α of the phenomenological relation is obtained from the semi-log plot of log $\dot{\varepsilon}$ versus time (Figure 14). Data presented by Singh and Mitchell (1968) indicate that the stress-intensity effect on the log of creep rate $\dot{\varepsilon}$ is linear over some intermediate stress intensity level; 30% to 90% is suggested. The calcareous ooze data presented in Figure 14 do not provide strong support for the linearity hypothesis. However, straight line curves were fitted to the data at various intervals of time. The relationships found for t = 50, 100, and 1,000 min were found to be near parallel, with an average slope α of 0.00427.

The parameter A, determined graphically, is 0.174%/min for this drained calcareous ooze data.

The desired expression for the creep strain function for the drained calcareous ooze tests was then evaluated as:

$$\varepsilon - a = -2.18(10^{0.00427x\bar{D}})t^{-0.080}$$

This relationship was then used to develop the calculated creep curves plotted in Figure 12 for creep shear loadings $\bar{D}$ of 34%, 55%, 69% and 80%. Note that the constant of integration "a" is used to adjust the creep curve up or down to fit any desired reference value; the calculated creep curves have been forced to fit measured creep data at times t of 0.1 or 0.5 min, as available. The calculated creep relationship does do a reasonably good job of duplicating the creep behavior of those specimens at the higher creep shear loadings $\bar{D}$ of 60% and 80%. This agreement exists largely because of the good straight line fit of these test data on the log $\dot{\varepsilon}$ versus log t plot (Figure 13); i.e., the data are well represented by the assumed relationship. Data developed from the other test specimens subjected to creep load intensities $\bar{D}$ of 34% and less are not represented well by the calculated creep relationship because the initial strain rates are far lower than predicted by the relationship.

The creep strain function evaluated to represent the drained behavior at 70% of ultimate deviator load indicates that the net creep strain will be about 3% after 20 yr. There appears to be no problem of creep failure for specimens loaded as high as 80% of the deviator load, for this calcareous ooze consolidated to 38 kPa. Further, if no impediment to drainage exists, then specimens consolidated to higher consolidation pressures should similarly not fail in creep.

Undrained Creep

Figures 15, 16 and 17 present axial strain versus logarithm of time results of the series of 9 undrained triaxial shear creep tests. Figure 15 presents data from specimens consolidated to about 38 kPa, the same consolidation pressure as that applied to the drained test series specimens. All three of these specimens were subjected to the full shear creep load

within a fraction of a minute. For these three tests, the time of load application is considered time zero for the presentation of the creep data. Note, in Figure 12 (drained creep) and in Figure 15 (undrained creep), that similar percentages of failure load correspond to quite different stress conditions and shear stress intensities. For example, at 70% of failure load, undrained specimen TC-16 was subjected to a principal stress difference $\bar{\sigma}_1$-$\bar{\sigma}_3$ of 30.7 kPa while drained specimen TC-10 was subjected to 72.4 kPa. The rather great differences in the strain magnitudes are due to the volume changes occurring in the drained specimens during shearing. The strain rates of the undrained specimens after some 1,000-min creep duration are noted to be very similar or slightly greater than those of the drained specimens at similar shear stress intensities. However, the shape of the undrained specimen creep curves is quite different from that of the drained specimens. The drained creep plots indicate a decreasing creep rate on a logarithm time plot; the undrained creep plots definitely suggest an increasing creep rate. In fact, with a relationship evaluated by Beard (1974) the undrained creep strain over 20 yr duration, for specimens consolidated to 38 kPa and loaded to 70% of maximum deviator load, is predicted to be 10.2% (versus 3% for drained specimens).

Figure 16 presents data from undrained creep tests on specimens consolidated to 15 kPa, a consolidation pressure less than half of that applied to the first group of specimens. Again, the same large differences in total strain are noted between the undrained specimens and the drained specimens of Figure 12. Again, the creep strain rates of the undrained specimens after some 1,000 min are noted to be very similar to, or slightly greater than, those of the drained specimens at similar stress intensities. However, the shape of the undrained creep curves of those specimens consolidated to 15 kPa is noted to be different from both previous sets of data: the data presented in Figure 16 shows a near constant strain rate on a logarithm of time scale, whereas strain rates for the drained tests decreased with time and strain rates for the set of undrained tests with $\bar{\sigma}_c$ = 38 kPa increased with time. With a second relationship evaluated by Beard (1974), the undrained creep

strain over 20 yr duration, for specimens consolidated to 15 kPa and loaded to 70% of maximum deviator load, is predicted to be 4.6%. This predicted creep strain at 20 yr is less than half of that for the other set of undrained creep specimens loaded to the same creep stress intensities but consolidated to a higher pressure.

Figure 17 presents data verifying this trend with creep test data from a specimen consolidated to 110 kPa and then subjected to a creep load equal to 80% of the maximum deviator stress at that consolidation stress. This specimen clearly failed, reaching 20% axial strain about 65 min after application of the last of 15 load increments. Initially, it would appear that the consolidation pressure differences are responsible for the noted differences in creep behavior. However, it is possible that, at least to some extent, the differences in creep behavior are due to the differing states of overconsolidation of the specimens, as noted by the stress-path curves of Figure 10. Creep test TC-3 with $\bar{\sigma}_c$ = 110 kPa does bring out the fact that specimens of this calcareous ooze can fail when subjected to only 80% of maximum deviator load; further, judging from the short time to reach failure for this specimen, it is possible that a similarly consolidated specimen loaded to 70% of maximum deviator load will also fail.

SUMMARY AND CONCLUSIONS

1. The sediment tested is termed a calcareous ooze on the basis of its carbonate content, is classified as a sandy clay according to the Trilineal Oceanic Soil Classification System (Richards, 1962), and behaves (in an engineering sense) as an inorganic silt according to the Unified Soil Classification System (Anon., 1968).

2. Because of its silty nature the calcareous ooze material is very susceptible to densification when subjected to vibration during transport; yet isolation from vibration is not practical. Therefore,

calcareous ooze samples must be examined and tested to the fullest extent possible onboard ship immediately after acquisition to minimize the degree of sample change between the as-measured and insitu states.

3. The calcareous samples completed primary consolidation in 1-D compression tests rapidly yielding coefficients of consolidation c_v from 0.002 cm^2/s at low pressures to 0.012 cm^2/s at high consolidation pressures.

4. Some of the compression curves e-log $\overline{\sigma}_v$ for these natural specimens do not straighten or flatten out at higher pressures as is normal; instead, the curves continue to plunge (i.e., the compression index $C_c = de/d(\log \overline{\sigma}_v)$, or slope of the curve, continues to increase). This phenomenon is believed due to the crushing of calcareous shells at higher pressures. Attempts at measuring or viewing evidence of such crushing were not successful. (It is also possible that this increased compressibility is being caused by large deformations of the hollow shells, but deformations short of crushing and puncturing.)

5. Crushing and puncturing of animal shells were noted when prepared (artificial) specimens consisting of the coarse (> no. 325 sieve) fraction were consolidated/compressed one-dimensionally. The e-log $\overline{\sigma}_v$ curves suggest that grain (or, in this case, shell) crushing is probably initiated at stresses of 50 to 200 kPa (7 to 28 psi). This coarse fraction proved considerably more compressible than the whole (natural) specimen, with a compression index C_c of 1.68 for the coarse fraction versus a C_c of 0.75 for the natural specimen. The fines in the natural specimen appear to serve as a stress distributing agent, loading the surfaces of the intact shells more evenly and limiting point-to-point contact between shells.

6. For the deep ocean calcareous ooze tested, the use of backpressuring during 1-D consolidation tests did not appear to produce improved results over those from nonbackpressured tests.

7. The angle of internal friction $\bar{\phi}$ for the calcareous ooze is about 0.60 rad (34.5 deg) for specimens subjected to effective lateral stresses up to about 30 kPa (4 psi). As the effective lateral stresses are increased from this value, the angle of internal friction decreases to about 0.49 rad (28 deg). Such change in behavior is believed due to the initiation of grain (shell) crushing at the higher effective stresses.

8. The phenomenological equation of Singh and Mitchell (1968), used to describe the calcareous ooze creep data presented, properly describes that data at high shear stress levels (50% to 80% of failure load). The equation is somewhat less descriptive at intermediate and low creep stress levels. However, at these lower creep stress levels, the equation overestimates the predicted creep strain. Such overestimation is conservative; therefore, use of the phenomenological relationship for stress levels to 80% is appropriate.

9. Shear creep failure of this calcareous deep ocean sediment does not appear to be a serious engineering problem. Specimens consolidated to simulate material 10 m below the seafloor and then allowed to drain during creep shear at 70% of failure indicate that only 3% creep strain will be experienced over 20 yr. Similar specimens not allowed to drain during creep shear at the same percentage loading indicate that 10% creep strain will be experienced over 20 yr. Such creep strain magnitudes are not serious. However, it appears likely that more highly consolidated specimens subjected to the same 70% of failure but to much higher shear stress magnitudes may experience creep failure at that loading.

ACKNOWLEDGMENTS

The assistance received in this endeavor is gratefully acknowledged: ship time and space, Naval Oceanographic Office; spade-box corer, Mr. Neil Marshall of Scripps Institution of Oceanography; officers and men of the USNS WILKES, (especially Captain William Barkmann, First Officer

Joseph Flaherty, and Boatswain Patrick Browning); scientific party on the WILKES (especially Mr. Frank Anderson, senior Naval Oceanographic Office representative); CEL technicians, Mr. Fred O. Lehnhardt and Mr. Leonard Woloszynski; and patient critic, Mr. Homa J. Lee.

REFERENCES

Altschaeffl, A. G. (1973) Personal communication, Associate Professor, School of Civil Engineering, Purdue University, Lafayette, Ind., Jun 1973.

Anon. (1968) Earth manual, Department of the Interior, Bureau of Reclamation, Denver, Colo., pp. 1-18.

Anon. (1971) Soil mechanics, foundations, and earth structures, Naval Facilities Engineering Command, Design Manual DM-7. Washington, D. C., Mar 1971, p. 7-3-12.

Beard, R. M. (1974) Unpublished status report: Development of an expedient site investigation tool and investigations in long-term anchor holding capacity, Civil Engineering Laboratory, Port Hueneme, Calif., May 1974, 44 pp.

Bryant, W. R., Delaflach, A. and Trabant, P., (1973) "Consolidation of marine clays," Deep-Sea Sediments: Physical and Mechanical Properties, edited by A. L. Inderbitzen. New York, N.Y., Plenum Press, pp 209-244.

Carrier, W. D., Bromwell, L. G. and Martin, R. T., (1973) "Behavior of returned lunar soil in vacuum," Journal of the Soil Mechanics and Foundations Division, ASCE, vol 99, no. SM11, Nov 1973, pp 979-996.

Einsele, G. (1967) "Sedimentary processes and physical properties of cores from the Red Sea, Gulf of Aden, and off the Nile Delta," Marine Geotechnique, edited by A. F. Richards. Urbana, Ill., University of Illinois Press, pp 154-169.

Herrmann, H. G., Rocker, Jr., K. and Babineau, P. H. (1972) Lobster and FMS: Devices for monitoring long-term seafloor foundation behavior, Naval Civil Engineering Laboratory, Technical Report R-775. Port Hueneme, Calif., Sep 1972, p. 41.

Hironaka, M. C. and Smith, R. J. (1967) "Foundation Study for Materials Test Structure," in Proceedings of Conference on Civil Engineering in the Oceans I, San Francisco, Calif., Sep 6-8, 1967, American Society of Civil Engineers, New York, pp 489-530.

Holmes, A. (1965) Principles of physical geology. New York, N.Y., Ronald Press Co., 1965, pp 847-855.

Keller, G. H. (1967) "Shear strength and other physical properties of sediments from some ocean basins," in Proceedings of Conference on Civil Engineering in the Oceans I, San Francisco, Sep 6-8, 1967, American Society of Civil Engineers, New York, pp 391-417.

Keller, G. H. (1969) "Mass properties of the sea floor in a selected depositional environment," in Proceedings of Conference on Civil Engineering in the Oceans II, Miami Beach, Fla., 1969, pp 857-877.

Lambe, T. W. and Whitman, R. V. (1969) Soil mechanics. New York, N.Y., John Wiley and Sons, 1969, pp 74, 105-115, 297, 302, 318, 421.

Lisitzin, A. P. (1971) "Distribution of carbonate microfossils in suspension and in bottom sediments," The Micropalaeontology of the Oceans, B. M. Funnel and W. R. Riedel, ed. London, England, Cambridge University Press, 1971, pp 202-203.

Marsal, R. J. (1967) "Large scale testing of rockfill materials," Journal of the Soil Mechanics and Foundations Division, ASCE, vol 93, no. SM2, Mar 1967, pp 27-43.

Mesri, R. (1973) "Coefficient of secondary compression," Journal of the Soil Mechanics and Foundations Division, ASCE, vol 99, no. SM1, Jan 1973, pp 123-127.

Miller, D. G. and Richards, A. F. (1969) "Consolidation and sedimentation - compression studies of a calcareous core, Exuma Sound, Bahamas," Sedimentology (Amsterdam), vol 12, no. 3-4, Jun 1969, pp 301-316.

Noorany, I. (1971) "Engineering properties of submarine calcareous soils from the Pacific," in Proceedings of International Symposium on the Engineering Properties of Sea-Floor Soils and Their Geophysical Identification, 25 Jul 1971, Seattle, Wash., University of Washington, 1971, pp 130-139.

Noorany, I. and Gizienski, S. F. (1970) "Engineering properties of submarine soils: State-of-the-art review," Journal of the Soil Mechanics and Foundations Division, ASCE, vol 96, no. SM5, Sep 1970, pp 1735-1762.

Richards, A. F. (1962) Investigation of deep-sea sediment cores, II. Mass Physical properties, Navy Hydrographic Office, Technical Report TR-106. Washington, D. C., Oct 1962.

Richards, A. F. (1973) "Standardization of marine geotechnics symbols, definitions, units, and test procedures," Deep-Sea Sediments: Physical and Mechanical Properties. New York, N. Y., Plenum Press, 1973, pp 271-292.

Roberts, J. E. (1964) Sand compression as a factor in oil field subsidence, Ph. D. thesis, Massachusetts Institute of Technology. Cambridge, Mass., 1964, 306 pp.

Rosfelder, A. M. and Marshall, N. F. (1967) "Obtaining large, undisturbed and orientated samples in deep water," Marine Geotechnique, A. F. Richards, ed. Urbana, Ill., University of Illinois Press, 1967, pp. 243-263.

Singh, A. and Mitchell, J. K. (1968) "General stress-strain-time function for soils," Journal of the Soil Mechanics and Foundations Division, ASCE, vol 94, no. SM1, Jan 1968, pp 21-46.

Singh, A. and Yang, Z. (1971) "Secondary compression characteristics of a deep ocean sediment," in Proceedings of International Symposium on the Engineering Properties of Sea-Floor Soils and Their Geophysical Identification, 25 Jul 1971, Seattle, Wash., University of Washington, 1971, pp 121-129.

Sverdrup, H. U., Johnson, M. W., and Fleming, R. H. (1942) The oceans. Englewood Cliffs, N. J., Prentice-Hall, 1942, pp 946-992.

Taylor, D. W. (1948) Fundamentals of soil mechanics. New York, N. Y., John Wiley and Sons, 1948, pp 217, 238-242.

Terzaghi, K. and Peck, R. B. (1968) Soil mechanics in engineering practice, 2nd ed., New York, N. Y., John Wiley and Sons, 1968, p. 73.

Terzaghi, R. (1940) "Compaction of lime mud as a cause of secondary structure," Journal of Sedimentary Petrology, vol 10, no. 2, Aug 1940, pp 78-90.

Valent, P. J. (1974) Short-term engineering behavior of a deep-sea calcareous sediment, Civil Engineering Laboratory, Technical Note N-1334. Port Hueneme, Calif., Mar 1974, p. 35.

Table 1. Sample Properties

Property Measured	Site 1	Site 2
Bulk density		
Immediately after sampling, Mg/m^3	1.46	1.45
After transport to laboratory, Mg/m^3	1.47	1.47
Laboratory vane strength, kPa (Location in core)	4.7 - 9.2 (bottom) (top)	
Specific gravity	2.65 - 2.69	
Carbonate content, %	56 - 75	
Atterberg limits		
Liquid	66 - 70	
Plastic	42 - 57	

Table 2. One-Dimensional Consolidation Specimen Data

Test No. (units)	Box/Tube	Depth (mm)	$\bar{w}_o$ [a]	$\bar{e}_o$ [b]	$\Delta\bar{\sigma}_v/\bar{\sigma}_v$	C_c	C_R [c]
Natural Specimens							
C-1	4/1	0-50	106.6	2.83	0.7	0.77	0.032
C-2	4/5	0-40	106.6	2.90	1	0.89	0.062
C-4	4/1	360-400	105.2	2.97	2	0.75	0.079
C-5	3/5	0-40	108.7	3.00	1	*d*	*d*
C-6	3/5	40-80	97.7	*e*	1	*e*	*e*
C-7	3/6	80-100	97.1	2.61	1	0.70	0.059
C-8	3/6	100-120	103.2	2.67	2	0.64	0.076
Artificial Specimens							
C-3	–	–	146.5	3.52	2	1.82	0.030
C-9	–	–	158.2	4.14	2	1.54	0.039

[a] $\bar{w}_o$ = initial water content, corrected for salt.

[b] $\bar{e}_o$ = initial void ratio, corrected for salt.

[c] C_R = rebound index.

[d] Not available, test halted early due to malfunction of temperature control.

[e] Not available, test halted early due to misalignment of apparatus.

Table 3. Measured and Calculated Values of Compression Index

Parameter Source	Value
Measured	
Range, C_c	0.89 to 0.64
Average, C_c	0.75
Calculated Empirical Relationship	
$C_c = 0.009 (w_L - 10)$[a]	0.52
$C_c = 0.011 (w_L - 12)$[b]	0.62
$C_c = 0.54 (e_o - 0.35)$[c]	1.27
$C_c = 0.0054 (2.6w - 35)$[c]	1.18

[a] Terzaghi and Peck (1968).

[b] Herrmann et al. (1972).

[c] Anon. (1971, p. 7-3-12).

Table 4. Triaxial Shear Strength Specimen Data

Test No. (units)	Box/Tube	Depth (mm)	$\bar{w}_o$ (%)	$\bar{e}_o$	$\bar{\sigma}_c$ (kPa)	$(\bar{\sigma}_1-\bar{\sigma}_3)_f$ [a] (kPa)	ε_f [a] (%)
CIU Tests – Sheared Undrained							
T-1	4/1	50-150	88.6	2.30	37.9	38.2	7.6
T-2	4/5	40-120	95.9	2.49	6.5	15.7	3.8
T-3	4/4	0-110	99.9	2.60	109.8	84.6	7.1
T-4	4/3	100-205	95.2	2.47	15.1	25.3	8.0
T-10	*b*	*b*	120.5	3.14	85.8	73.11	6.9
CID Tests – Sheared Drained							
T-5	4/5	120-240	102.0	2.64	15.3	48.4	20
T-6	4/2	0-100	99.0	2.62	15.3	46.7	12.8
T-7	1/3	0-110	101.4	2.65	110.6	235	20
T-8	4/6	0-100	99.2	2.61	110.3	240	20
T-9	1/4	0-105	102.9	2.69	48.3	125.3	20

[a] Failure condition defined at $(\bar{\sigma}_1/\bar{\sigma}_3)_{max}$.

[b] Location of Specimen unknown.

Table 5. Triaxial Creep Specimen Data

Test No. (units)	Box/Tube	Depth (mm)	$\overline{w}_o$ (%)	$\overline{w}_f$[a] (%)	$\overline{e}_o$	$\overline{\sigma}_c$ (kPa)	$(\overline{\sigma}_1-\overline{\sigma}_3)_{creep}$ (kPa)	D (%)
CIU Tests – Undrained Shear and Creep								
TC-1	2/1	0-145	102.1	93.3	2.66	15.2	15.8	62
TC-2	4/1	150-250	103.5	97.1	2.69	6.48	25.2	90
TC-3	4/4	110-210	102.2	83.8	2.65	110.5	71.0	83
TC-4	4/3	0-100	96.8	93.4	2.55	15.0	17.8	70
TC-12	2/6	100-200	110.9	101.9	2.80	14.9	8.33	46
TC-13[b]	2/6[b]	100-200[b]	101.9[b]	92.2	2.56	37.9	12.6	38
TC-14	2/6	200-310	111.9	92.3	2.74	37.9	20.7	65
TC-15	2/5	0-100	102.9	94.6	2.72	15.2	15.2	74
TC-16[b]	2/5[b]	0-100[b]	94.6[b]	88.2	2.51	37.9	30.7	70
CID Tests – Drained Shear and Creep								
TC-5	1/6	0-100	102.4	94.1	2.68	38.1	30.3	29
TC-6	1/6	100-205	97.4	86.5	2.57	38.2	36.2	34
TC-7	1/6	205-305	110.7	93.8	2.90	37.8	21.6	20
TC-8	3/1	0-110	99.9	87.5	2.63	38.2	29.0	28
TC-9	3/2	0-110	100.8	84.0	2.66	38.4	58.2	55

continued

Table 5. continued

Test No. (units)	Box/Tube	Depth (mm)	$\bar{w}_o$ (%)	$\bar{w}_f$[a] (%)	$\bar{e}_o$	$\bar{\sigma}_c$ (kPa)	$(\bar{\sigma}_1-\bar{\sigma}_3)_{creep}$ (kPa)	D (%)
CID Tests – Drained Shear and Creep (continued)								
TC-10	3/2	180-280	111.6	87.5	2.94	38.1	72.4	69
TC-11	3/3	25-125	90.4	73.8	2.38	38.2	83.7	80

[a]Final water content, salt corrected.

[b]Creep specimen reconsolidated to 37.9 kPa after creep at 14.9 kPa and retested.

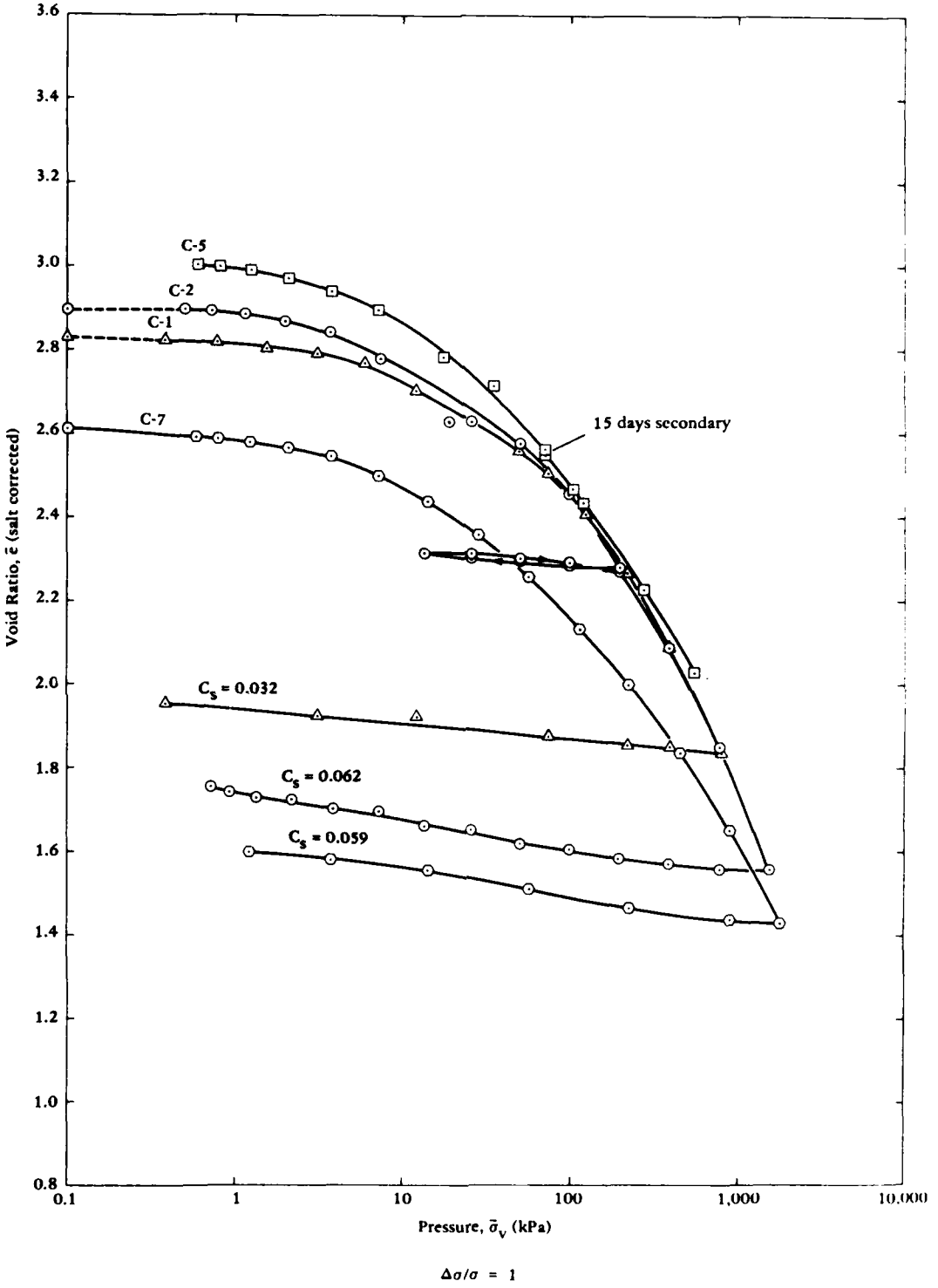

Figure 1. One-dimensional consolidation of n

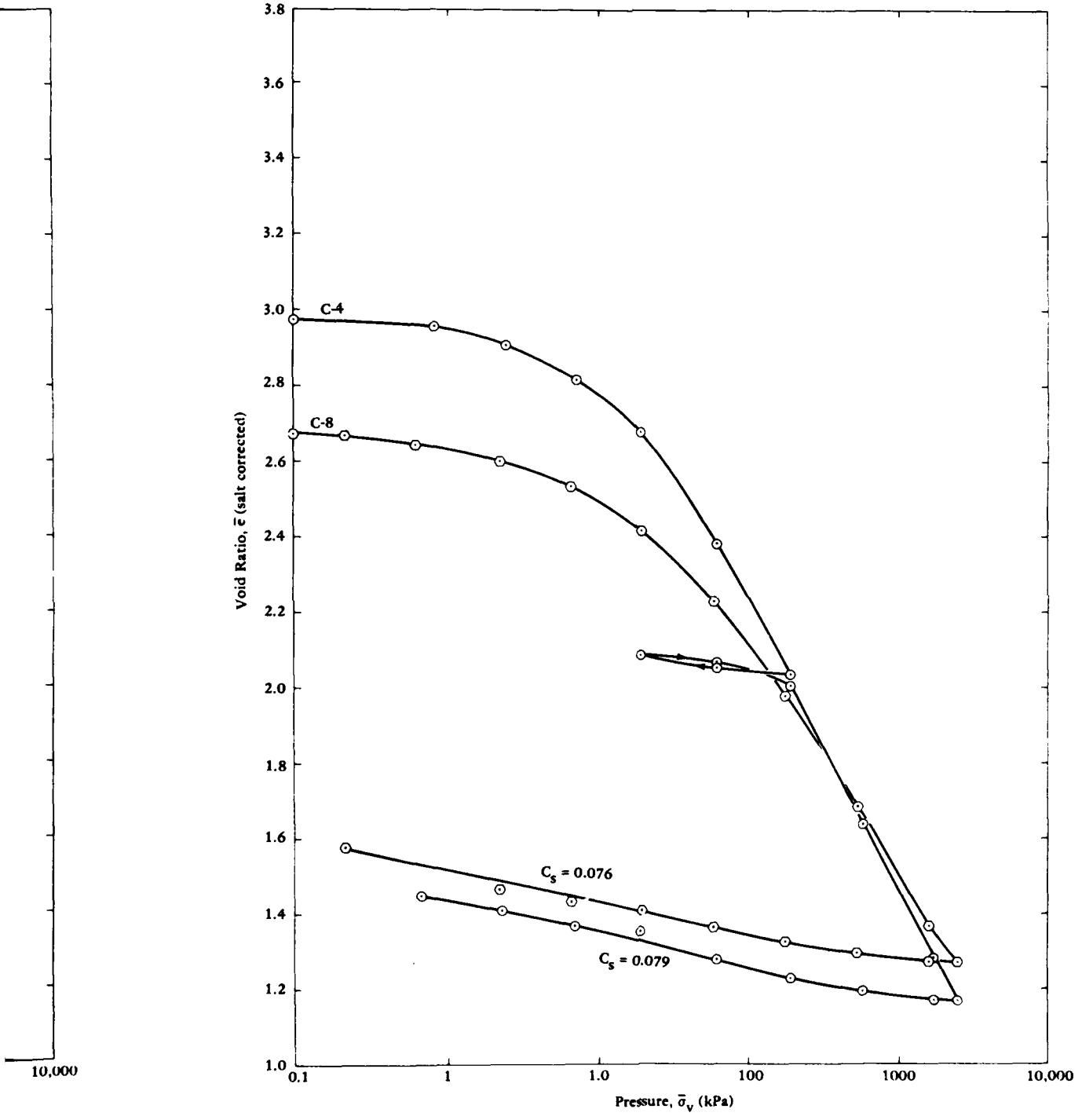

ional consolidation of natural specimens.

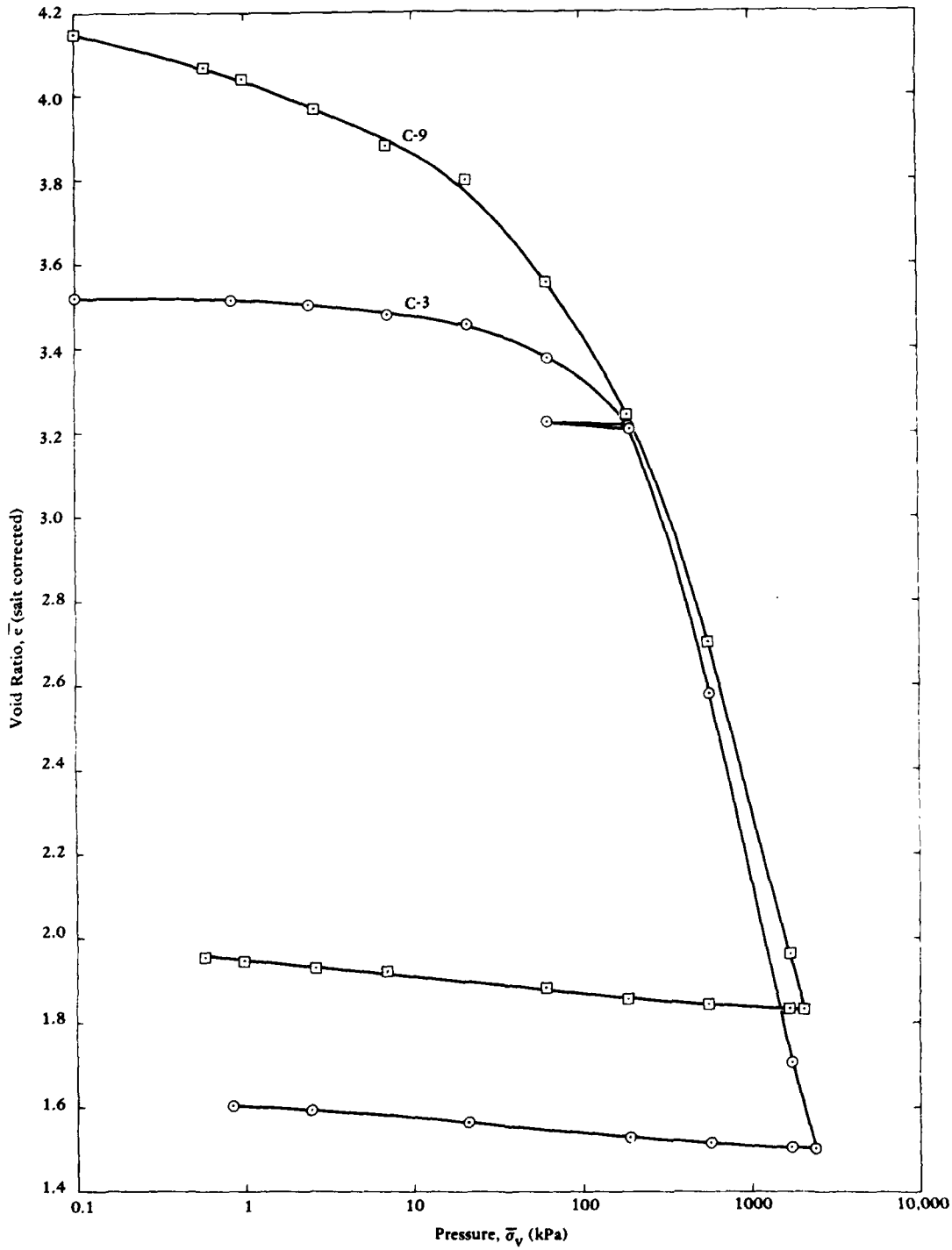

Figure 2. One-dimensional consolidation of artificial specimens.

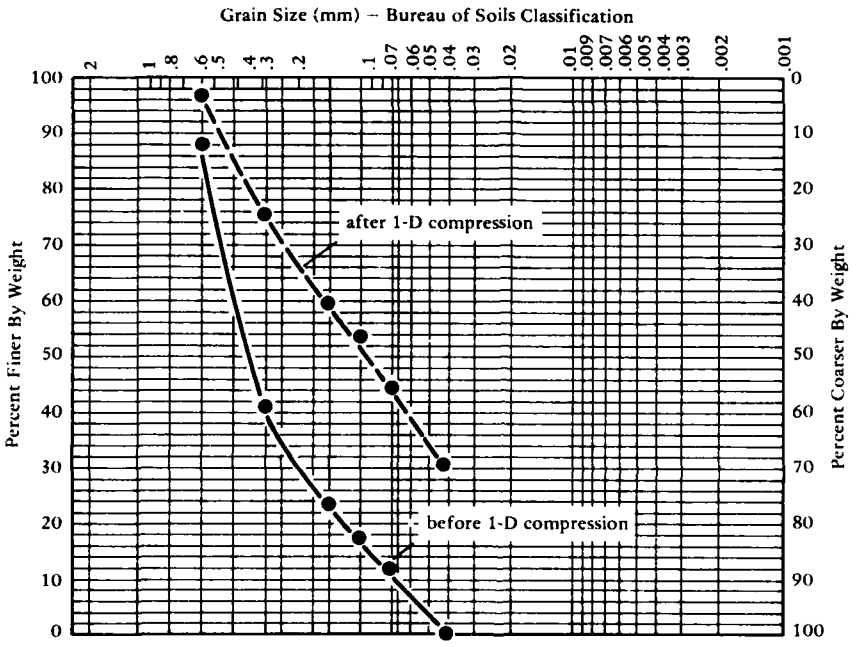

Figure 3. Grain size analysis results on artificial sample used in one-dimensional consolidation test C-3. Sample prepared from material retained on no. 325 sieve (0.043 mm).

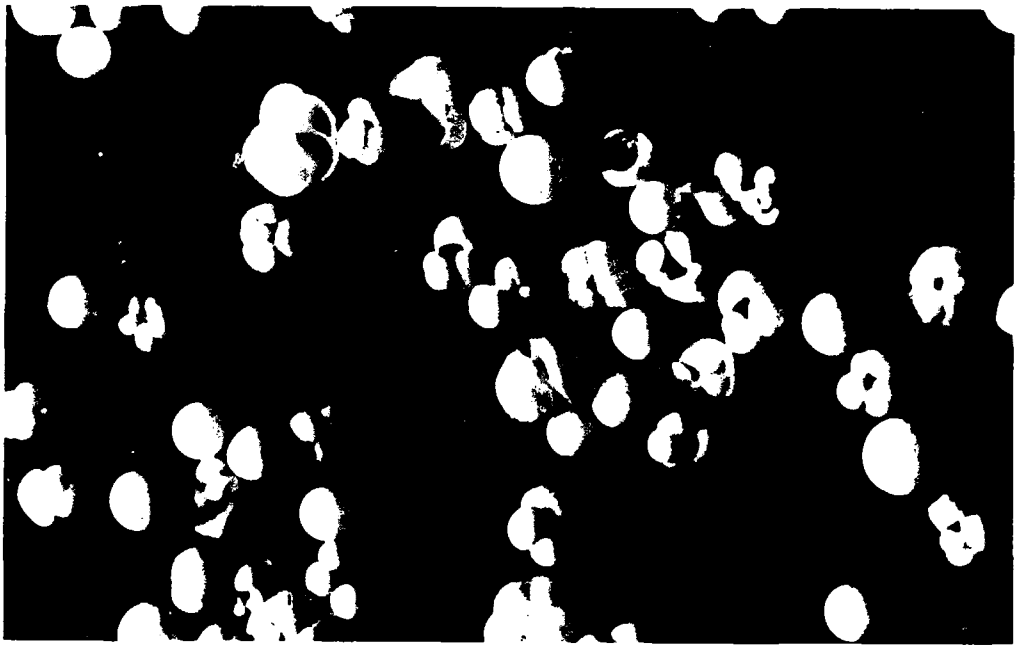

Figure 4. Fraction retained on no. 30 sieve, artificial sample, before 1-D compression (note that about 9% of spherical shells are broken).

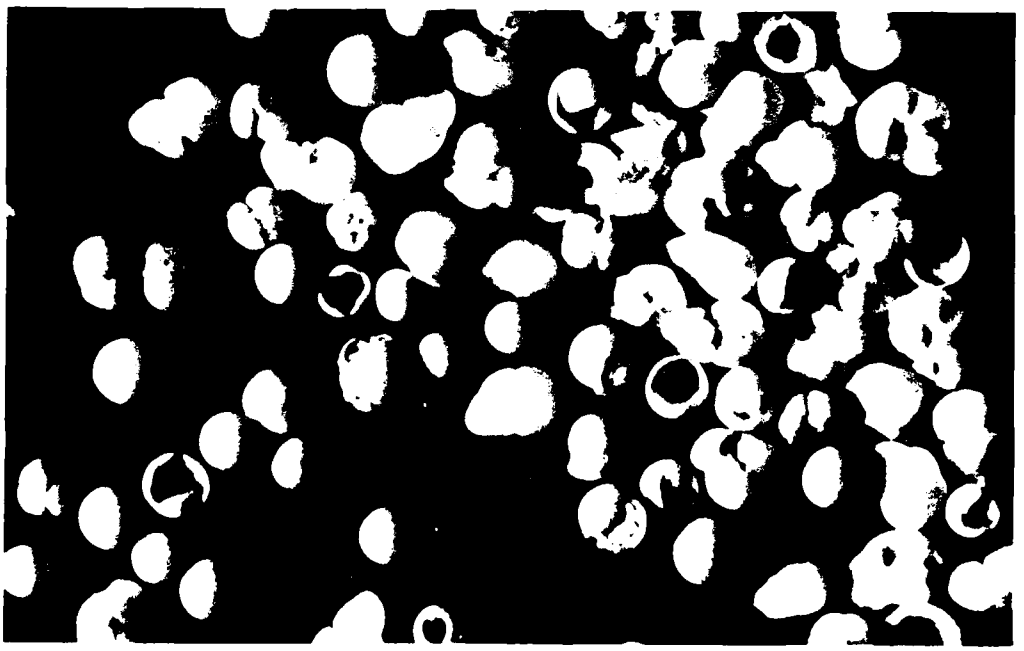

Figure 5. Fraction retained on no. 30 sieve, artificial sample, after 1-D compression (note that about 38% of spherical shells are broken).

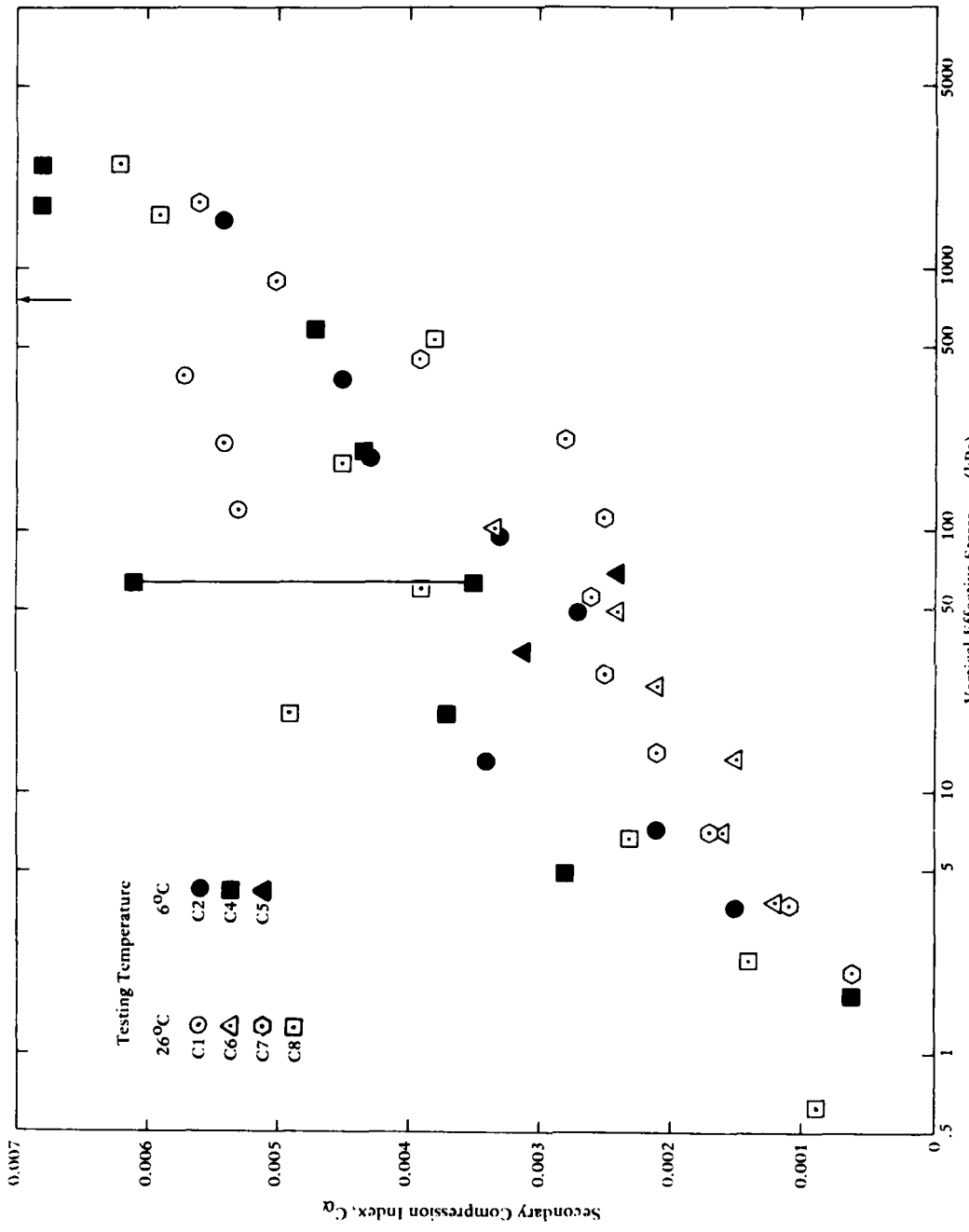

Figure 6. Effect of temperature on C_α.

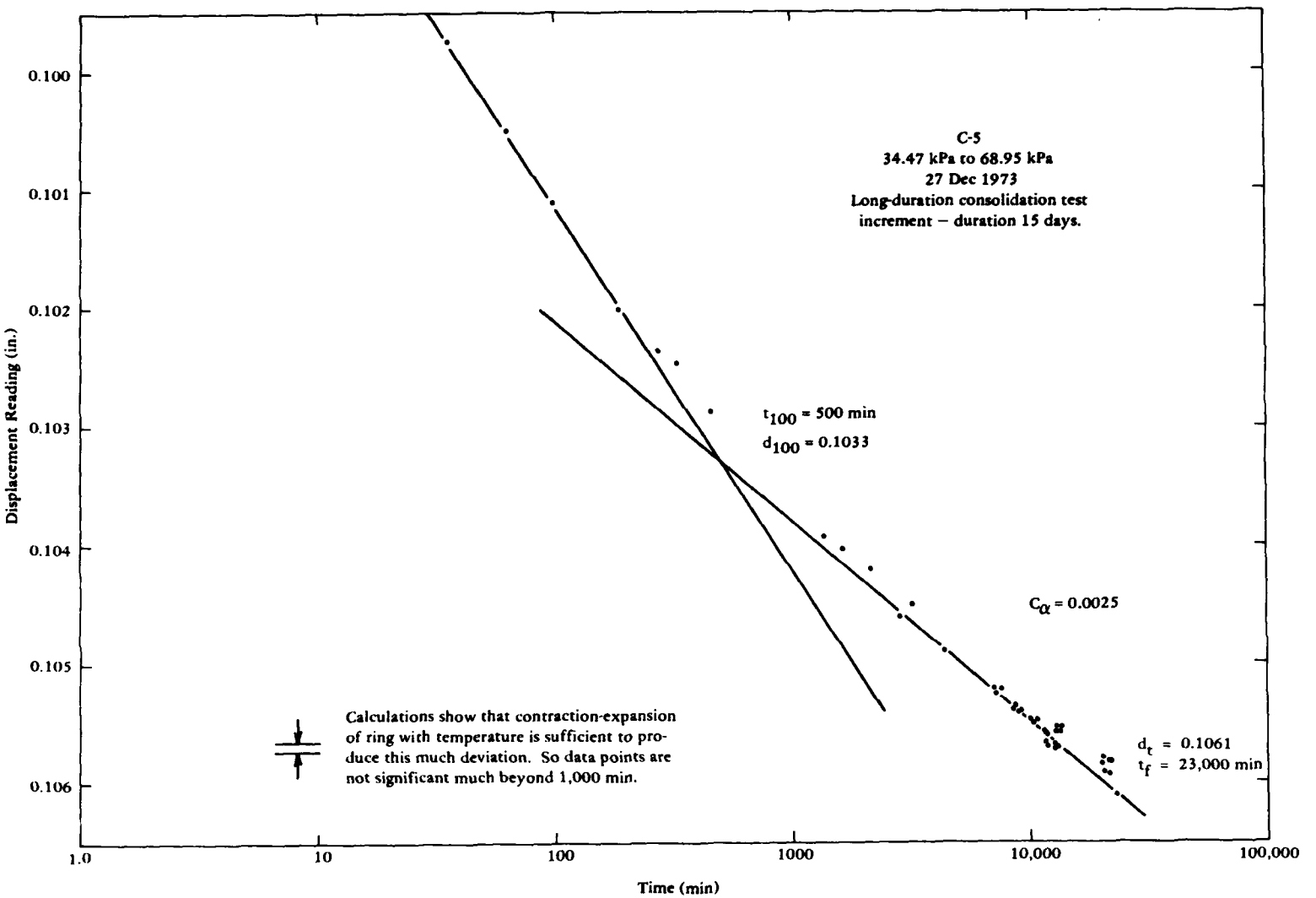

Figure 7. Long-duration, 1-D consolidation test increment.

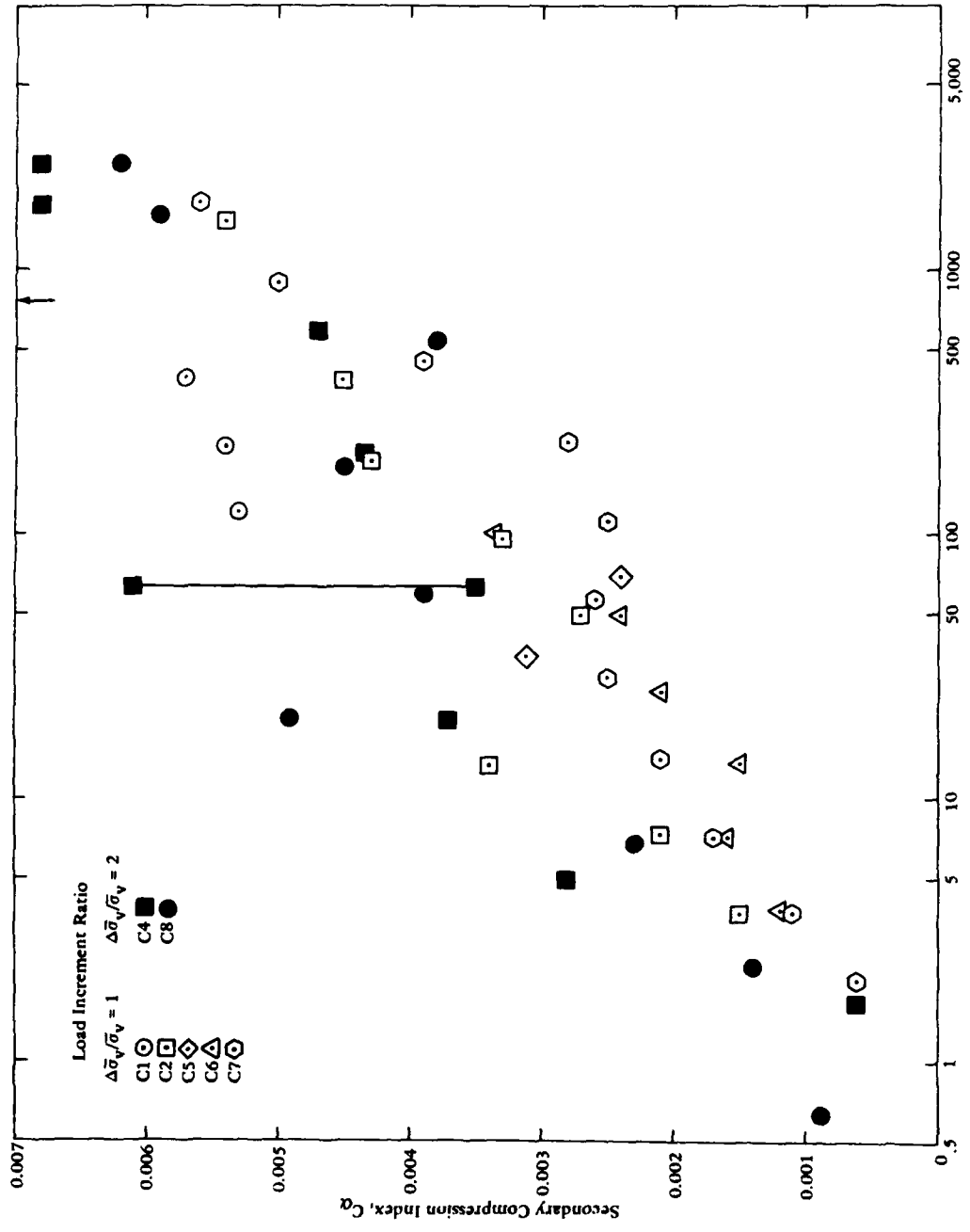

Figure 8. Effect of $\Delta\bar{\sigma}_v/\bar{\sigma}_v$ on C_α.

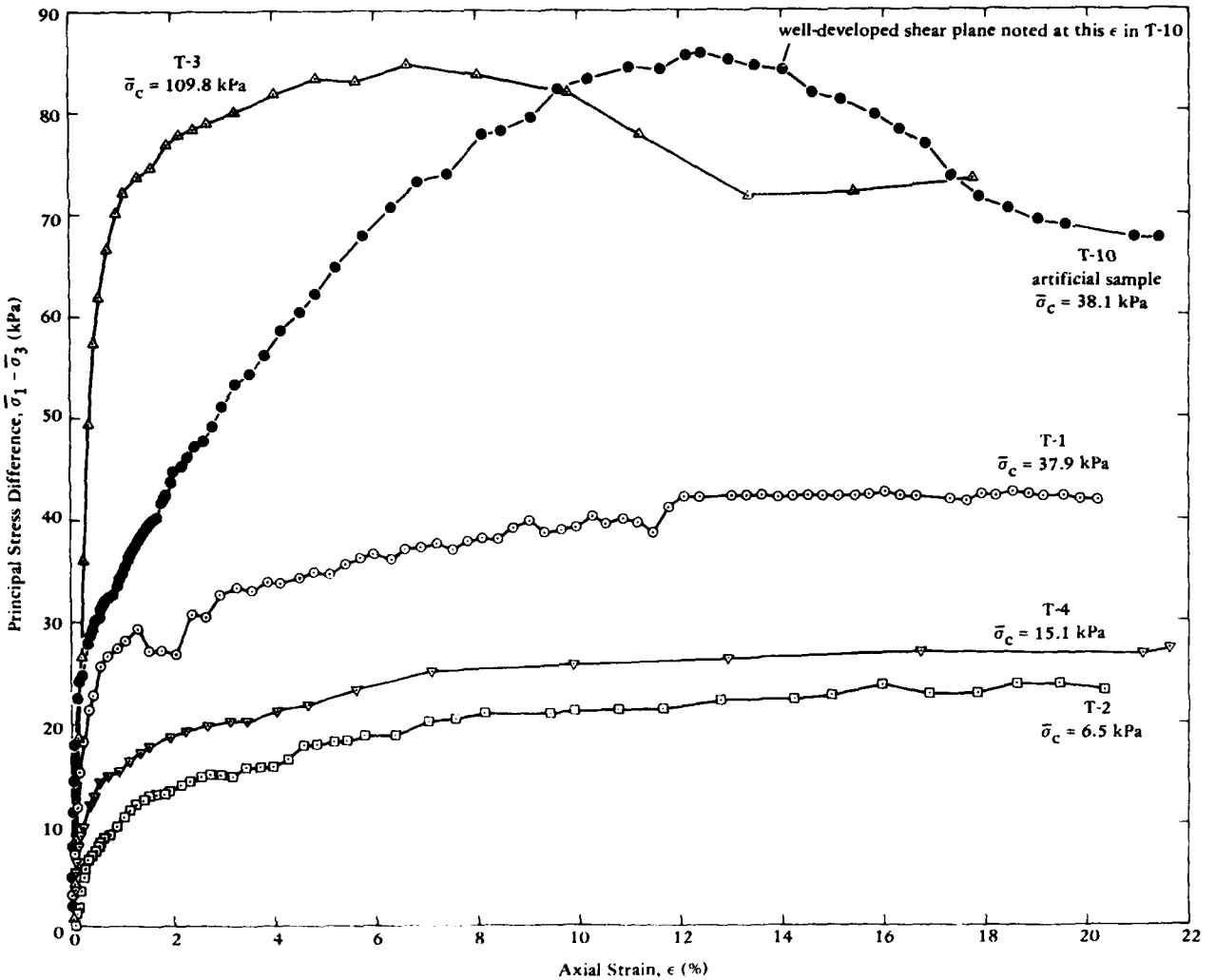

Figure 9. Stress-strain curves for CIU triaxial specimens.

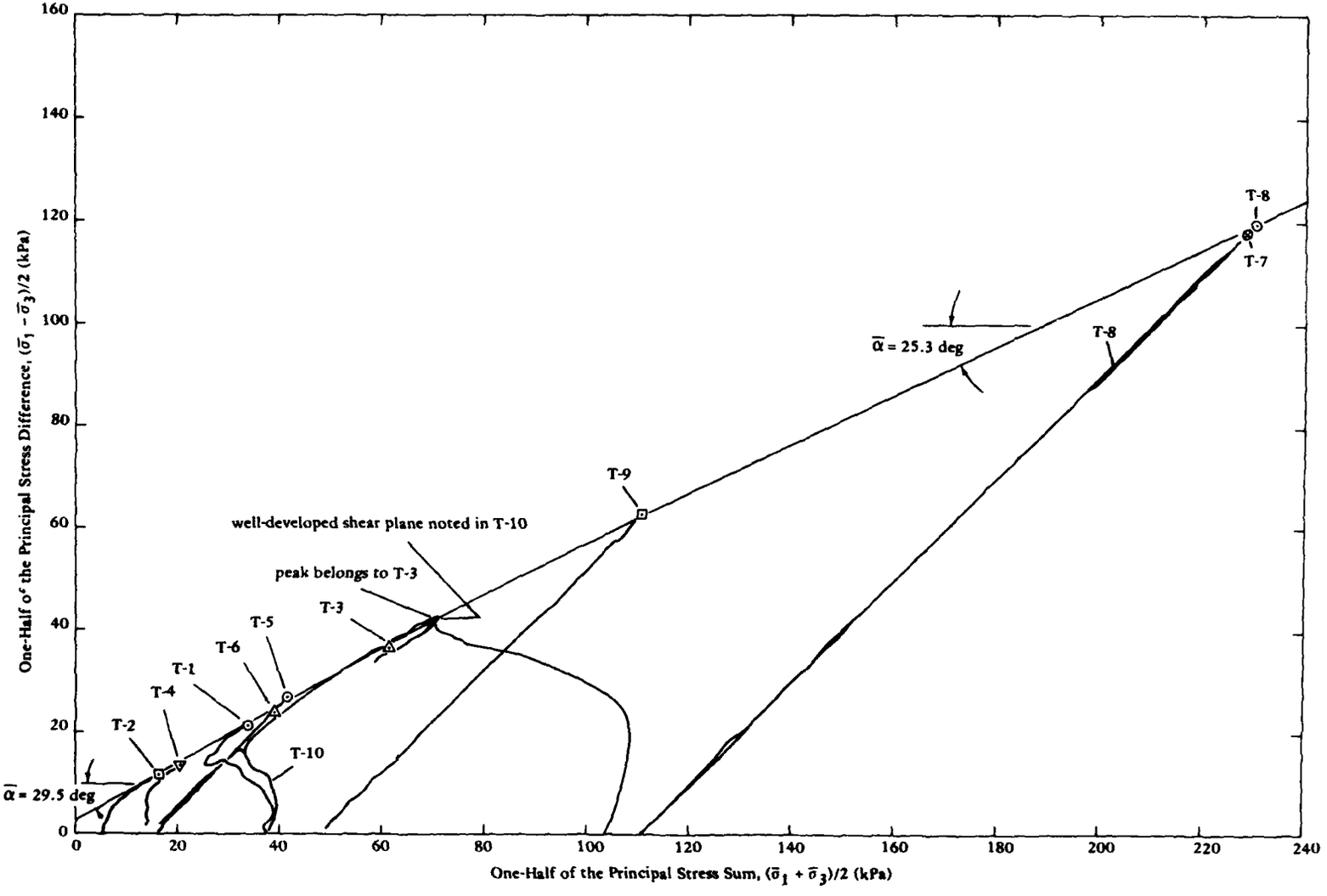

Figure 10. Stress path curves and failure envelope for CIU and CID triaxial specimens.

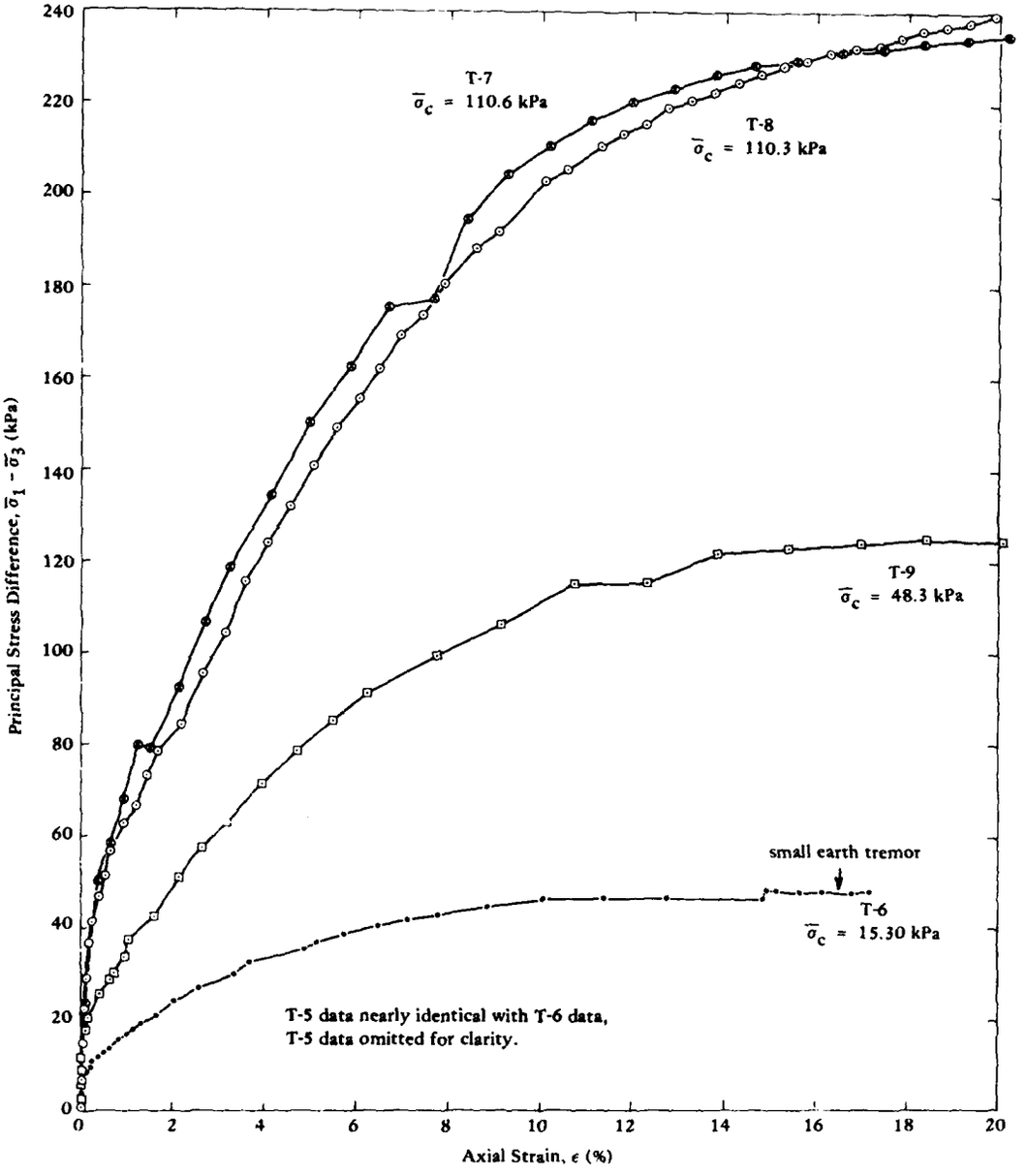

Figure 11. Stress-strain curves for CID triaxial specimens.

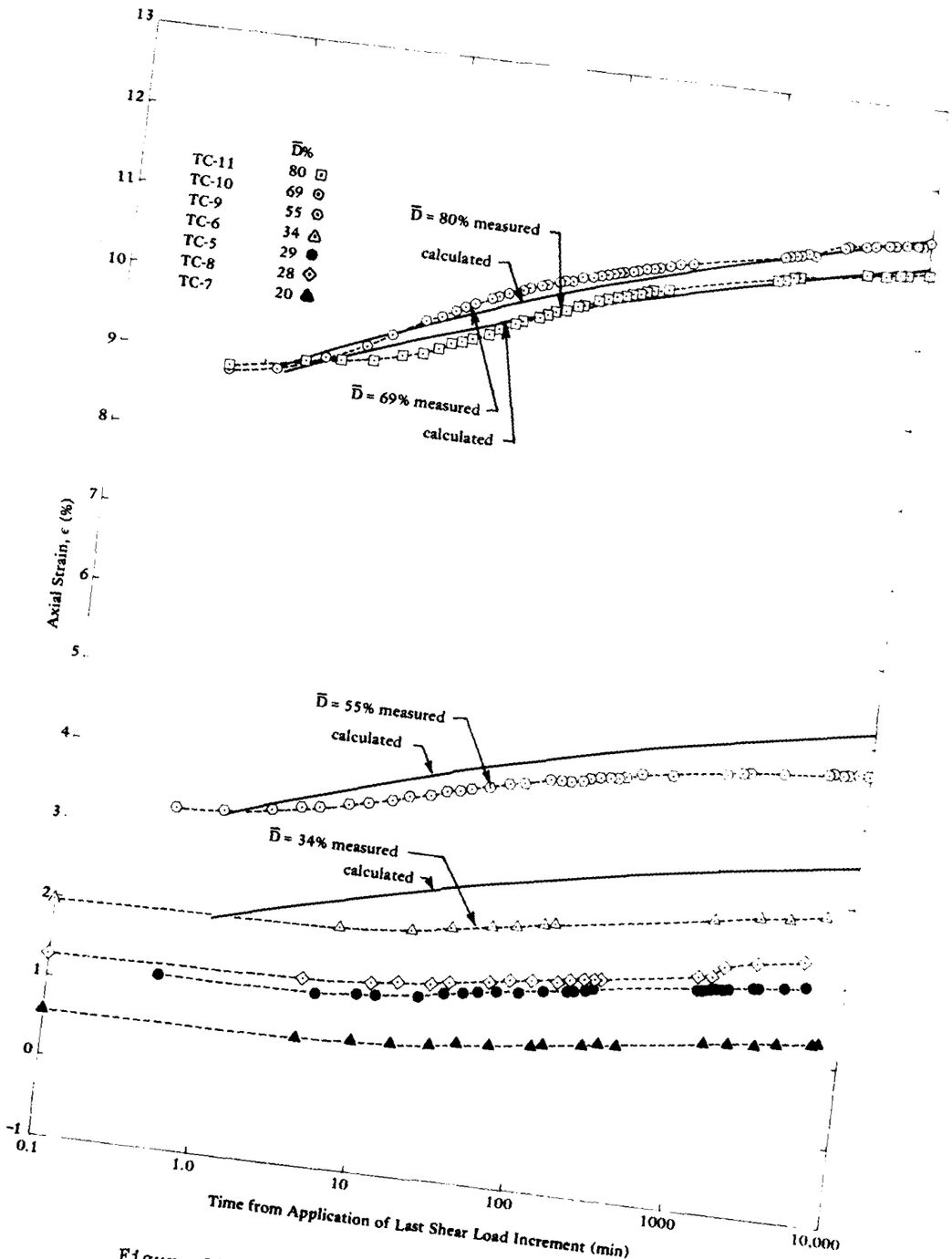

Figure 12. Creep of drained triaxial specimens.

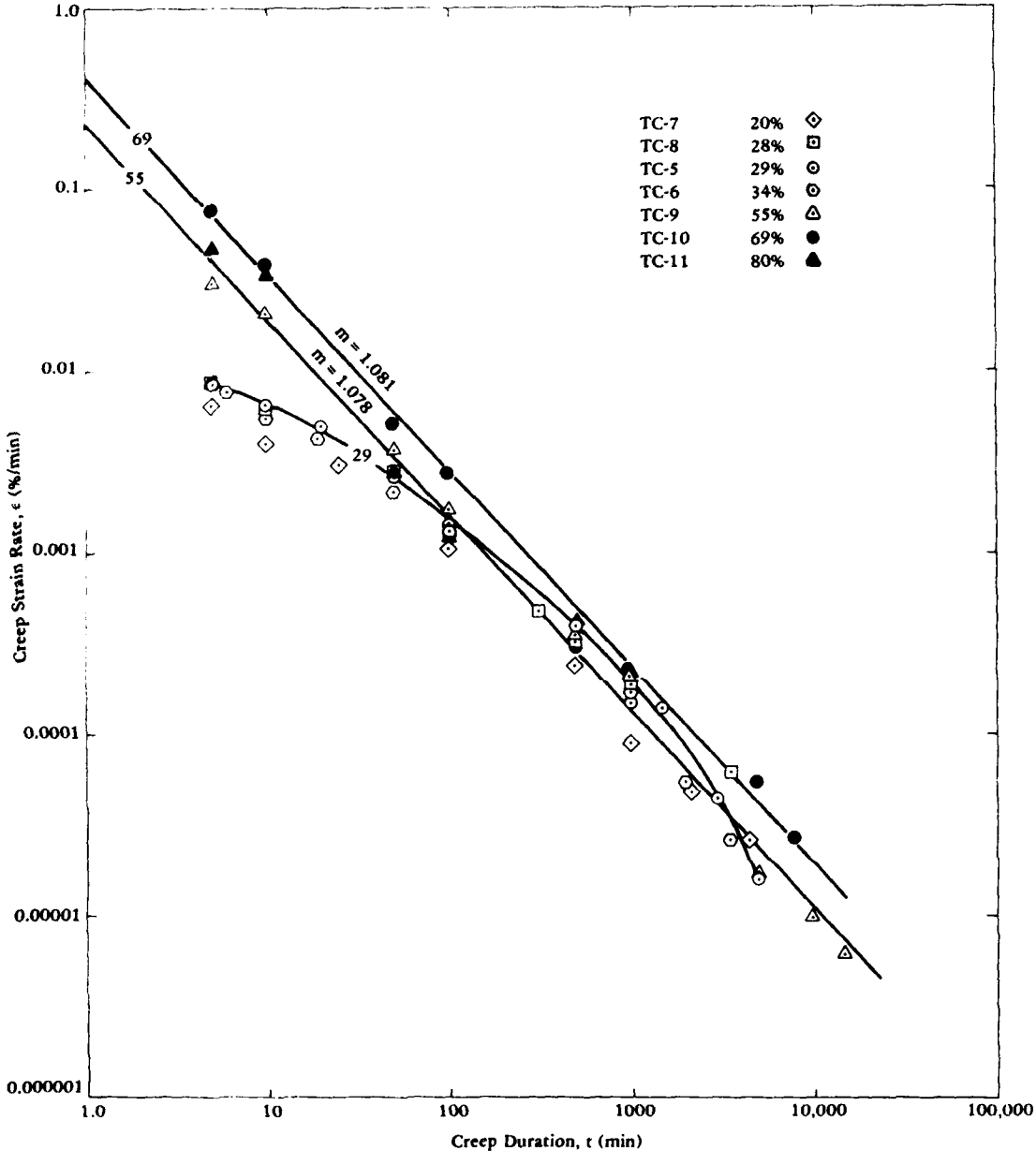

Figure 13. Comparison of creep strain rate versus time at different loading intensities.

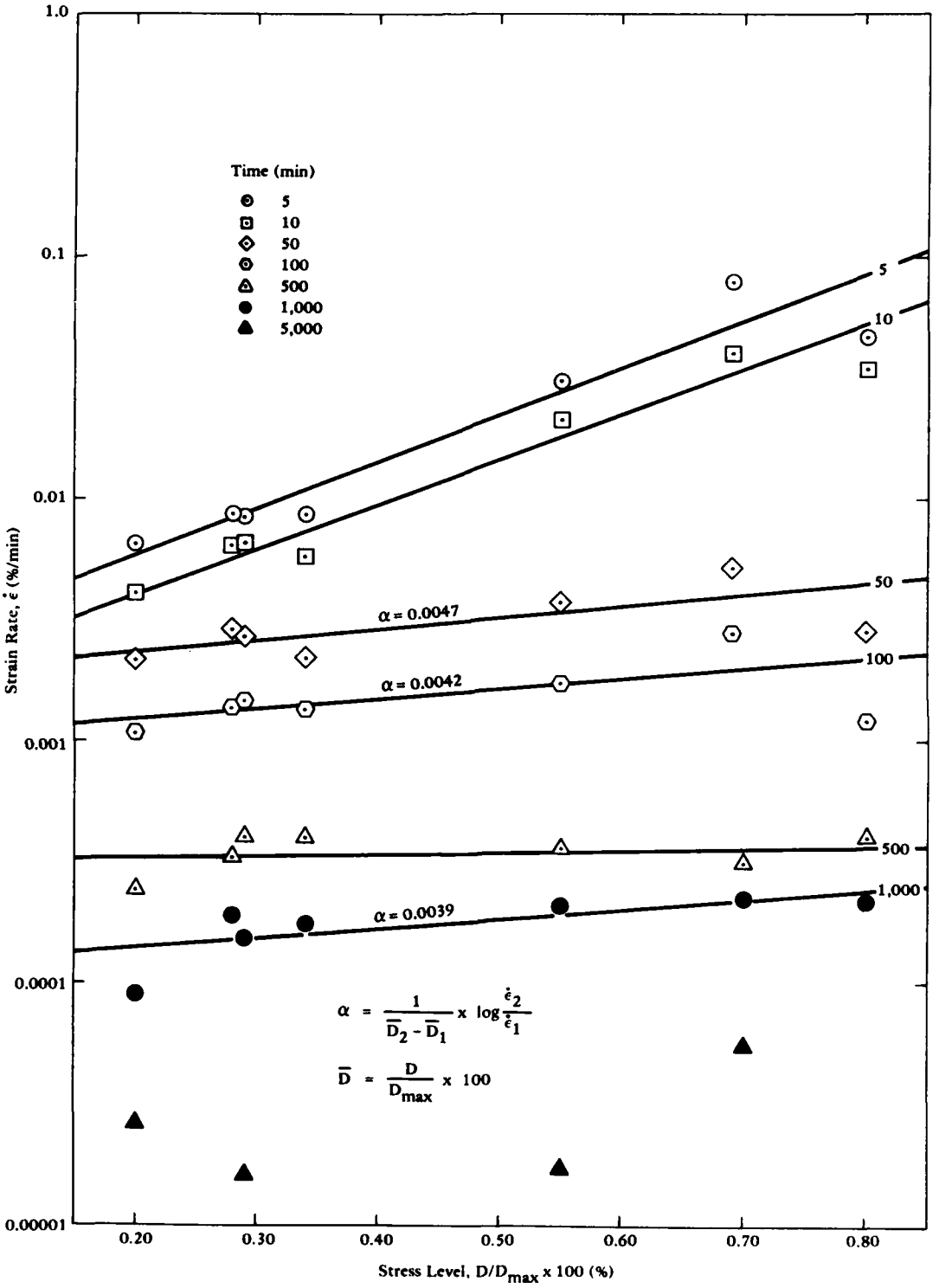

Figure 14. Comparison of creep strain rate versus loading intensity at different times.

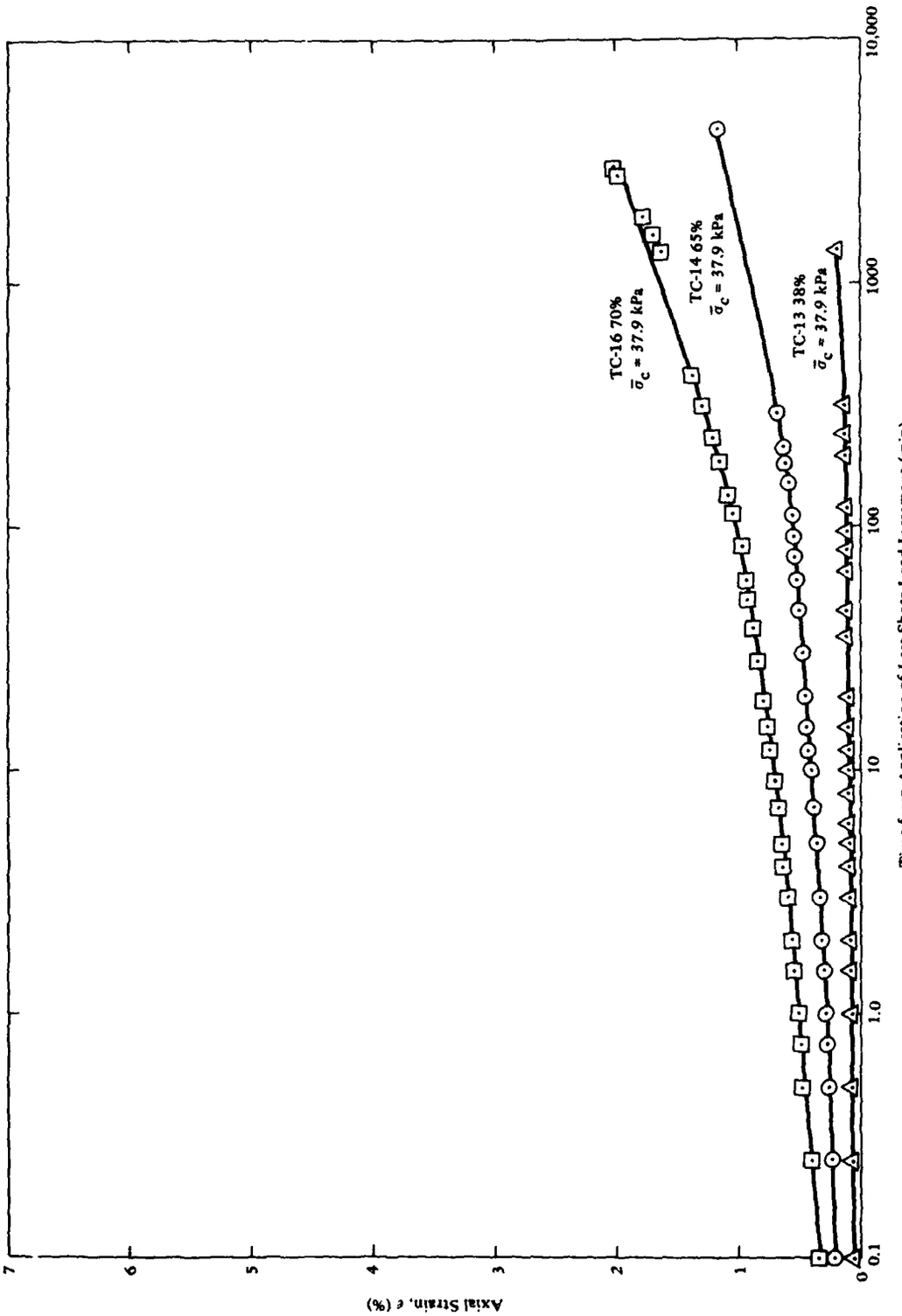

Figure 15. Creep of undrained triaxial specimens consolidated to 37.9 kPa.

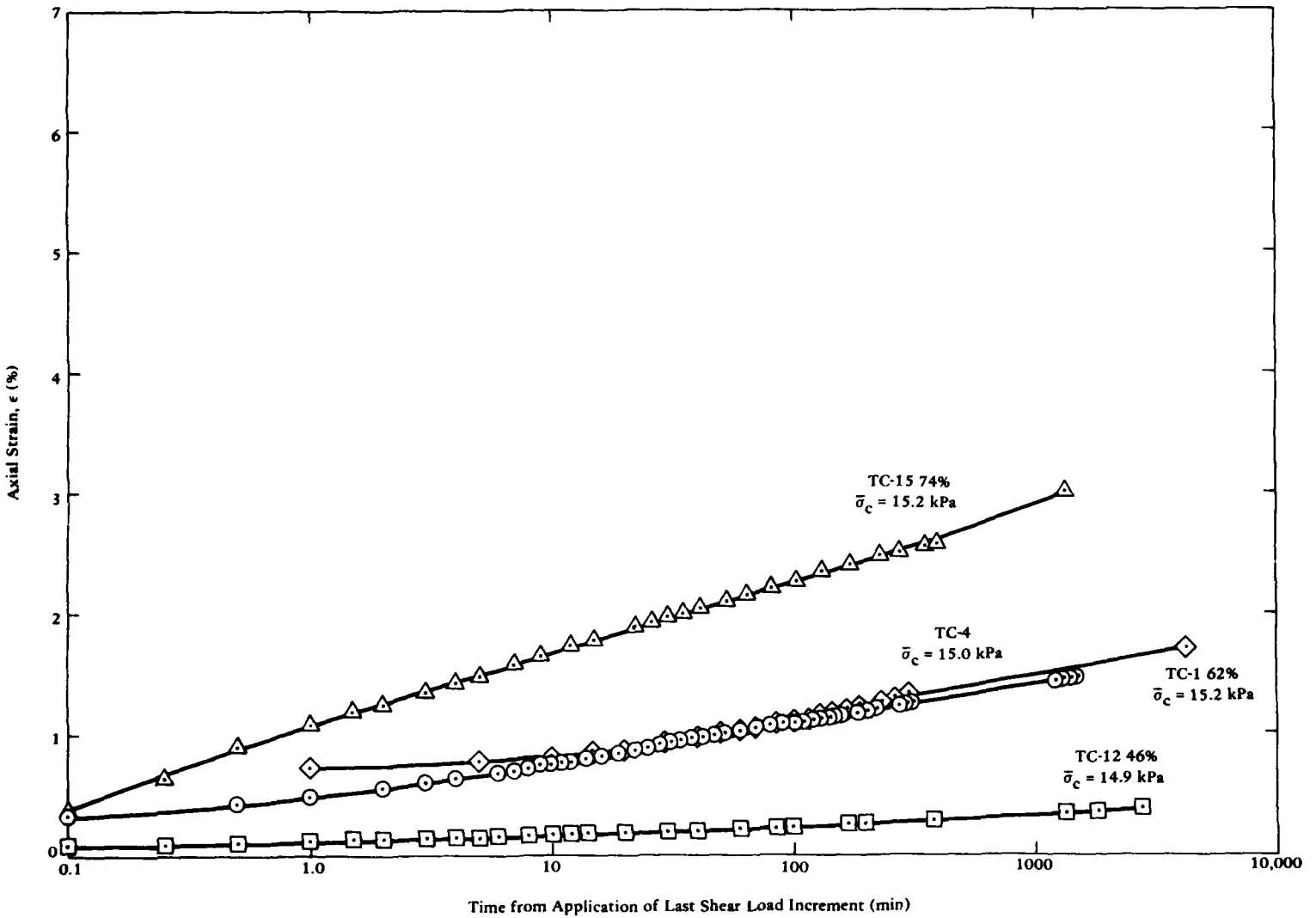

Figure 16. Creep of undrained triaxial specimens consolidated to 15.0 kPa.

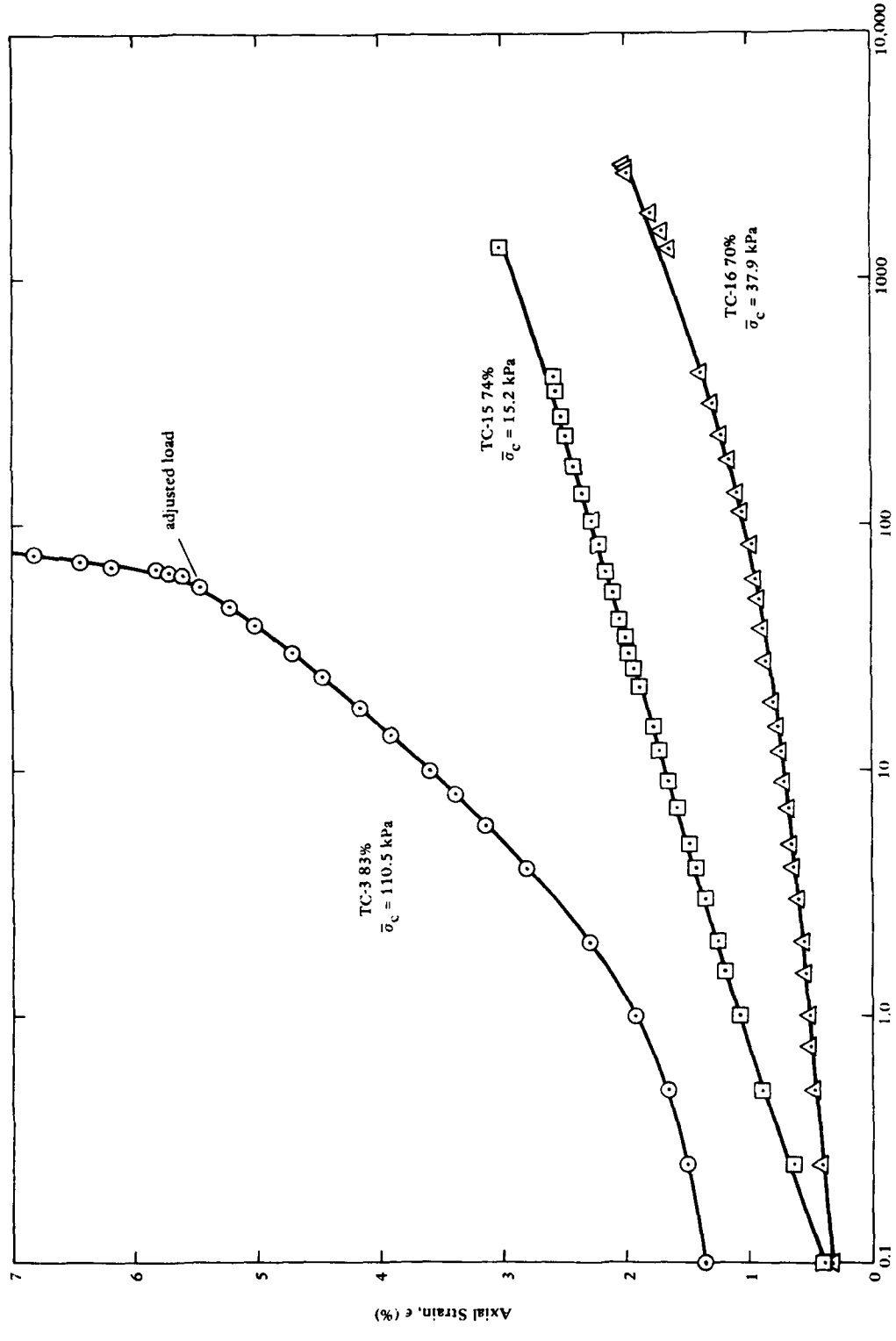

Figure 17. Creep of undrained triaxial specimens at similar load intensities.

DISTRIBUTION LIST

AFB CESCH, Wright-Patterson
ARMY BMDSC-RE (H. McClellan) Huntsville AL; DAEN-MCE-D Washington DC
ARMY COASTAL ENGR RSCH CEN Fort Belvoir VA; R. Jachowski, Fort Belvoir VA
ARMY CORPS OF ENGINEERS MRD-Eng. Div., Omaha NE; Seattle Dist. Library, Seattle WA
ARMY CRREL A. Kovacs, Hanover NH
ARMY ENG WATERWAYS EXP STA Library, Vicksburg MS
ARMY ENGR DIST. Library, Portland OR
ARMY ENVIRON. HYGIENE AGCY Water Qual Div (Doner), Aberdeen Prov Ground, MD
ARMY MATERIALS & MECHANICS RESEARCH CENTER Dr. Lenoe, Watertown MA
ARMY MOBIL EQUIP R&D COM Mr. Cevasco, Fort Belvoir MD
ASST SECRETARY OF THE NAVY Spec. Assist Energy (P. Waterman), Washington DC; Spec. Assist Submarines, Washington DC
BUREAU OF RECLAMATION Code 1512 (C. Selander) Denver CO
MCB ENS S.D. Keisling, Quantico VA
CINCLANT Civil Engr. Supp. Plans. Ofr Norfolk, VA
CNO Code NOP-964, Washington DC; Code OP 987 Washington DC; Code OPNAV 09B24 (H); Code OPNAV 22, Wash DC; Code OPNAV 23, Wash DC; OP987J (J. Boosman), Pentagon
COMOCEANSYSPAC SCE, Pearl Harbor HI
DEFENSE DOCUMENTATION CTR Alexandria, VA
DOE Dr. Cohen
HEDSUPPACT PWO, Taipei, Taiwan
HQFORTRPS 2nd FSCG, (Caudillo) Camp Lejeune, NC
MCAS Facil. Engr. Div. Cherry Point NC; J. Taylor, Iwakuni Japan
MCRD PWO, San Diego Ca
NAF PWO, Atsugi Japan
NAS Code 18700, Brunswick ME; Dir. Util. Div., Bermuda; ENS Buchholz, Pensacola, FL; PWD Maint. Div., New Orleans, Belle Chasse LA; PWO Belle Chasse, LA; PWO Key West FL; PWO, Glenview IL; SCE Norfolk, VA
NATL RESEARCH COUNCIL Naval Studies Board, Washington DC
NAVACT PWO, London UK
NAVAEROSPREGMEDCEN SCE, Pensacola FL
NAVAL FACILITY PWO, Barbados; PWO, Centerville Bch, Ferndale CA
NAVCOASTSYSLAB Code 715 (J. Mittleman) Panama City, FL; Library, Code 715 (J. Quirk) Panama City, FL
NAVCOMMAREAMSTRSTA PWO, Wahiawa HI; SCE Unit 1 Naples Italy
NAVCOMMSTA Code 401 Nea Makri, Greece; PWO, Exmouth, Australia
NAVEDTRAPRODEVCEN Tech. Library
NAVELEXSYSCOM Code PME-124-61, Washington DC
NAVENVIRHLTHCEN CO, Cincinnati, OH
NAVFACENGCOM Code 043 Alexandria, VA; Code 044 Alexandria, VA; Code 0451 Alexandria, VA; Code 0453 (D. Potter) Alexandria, VA; Code 0454B Alexandria, Va; Code 04B5 Alexandria, VA; Code 1023 (T. Stevens) Alexandria, VA; Morrison Yap, Caroline Is.; PC-22 (E. Spencer) Alexandria, VA; PL-2 Ponce P.R. Alexandria, VA
NAVFACENGCOM - CHES DIV, Code FPO-1 (C. Bodey) Wash, DC; Code FPO-1 (Ottsen) Wash, DC; Code FPO-1C2 Wash, DC; Code FPO-1P4 (Gregory); Code FPO-1SP (Dr. Lewis) Wash, DC; Code FPO-1SP13 (T F Sullivan) Wash, DC; Code FPO-1P12 (Mr. Scola), Washington DC; Scheessele, Code 402, Wash, DC
NAVFACENGCOM - LANT DIV.; RDT&ELO 09P2, Norfolk VA
NAVFACENGCOM - NORTH DIV. (Boretsky) Philadelphia, PA; CO; Code 1028, RDT&ELO, Philadelphia PA; ROICC, Contracts, Crane IN
NAVFACENGCOM - PAC DIV, Code 09DG (Donovan), Pearl Harbor, HI; Code 402, RDT&E, Pearl Harbor HI
NAVFACENGCOM - SOUTH DIV, Code 90, RDT&ELO, Charleston SC
NAVFACENGCOM - WEST DIV, Code 04B; 09P/20; RDT&ELO Code 2011 San Bruno, CA
NAVFACENGCOM CONTRACT Eng Div dir, Southwest Pac, Manila, PI; OICC, Southwest Pac, Manila, PI
NAVHOSP LT R, Elsbernd, Puerto Rico
NAVNUPWRU MUSE DET Code NPU80 (ENS W. Morrison), Port Hueneme CA
NAVOCEANO Code 1600 Bay St. Louis, MS; Code 3408 (J. Kravitz) Bay St. Louis
NAVOCEANR&DACT Code 450 Bay St. Louis MS

NAVOCEANSYSCEN Code 409 (D. G. Moore), San Diego CA; Code 4473 Bayside Library, San Diego, CA; Code 52 (H. Talkington) San Diego CA; Code 5224 (R.Jones) San Diego CA; Code 5311(T) (E. Hamilton) San Diego CA; Code 6505 (J. Stachiw), San Diego, CA; Code 6565 (Tech. Lib.), San Diego CA
NAVPGSCOL Code 61WL (O. Wilson) Monterey CA; D. Leipper, Monterey CA; E. Thornton, Monterey CA
NAVPHIBASE CO, ACB 2 Norfolk, VA; Code S3T, Norfolk VA; OIC, UCT ONE Norfolk, Va
NAVREGMEDCEN SCE (D. Kaye); SCE, Guam
NAVSCOLCECOFF C35 Port Hueneme, CA
NAVSEASYSCOM Code OOC (LT R. MacDougal), Washington DC
NAVSEC Code 6034 (Library), Washington DC;
NAVSHIPYD Code 440 Portsmouth NH; Code 440, Puget Sound, Bremerton WA; PWD (LT N.B. Hall), Long Beach CA; Salvage Supt, Phila., PA; Tech Library, Vallejo, CA
NAVSTA PWD (LTJG.P.M. Motolenich), Puerto Rico; PWO, Mayport FL; Utilities Engr Off. (LTJG A.S. Ritchie), Rota Spain
NAVSUPPACT Code 413, Seattle WA; LTJG McGarrah, Vallejo CA
NAVSURFWPNCEN PWO, White Oak, Silver Spring, MD
NAVTECHTRACEN SCE, Pensacola FL
NAVWPNCEN Code 2636 (W. Bonner), China Lake CA
NAVWPNSTA PW Office (Code 09C1) Yorktown, VA; PWO, Seal Beach CA
NAVWPNSUPPCEN Code 09 (Boennighausen) Crane IN
NAVXDIVINGU LT A.M. Parisi, Panama City FL
NCBC CEL (CAPT N. W. Petersen), Port Hueneme, CA; CEL AOIC Port Hueneme CA; Code 10 Davisville, RI
NOAA Libraries Div. - D823, Silver Spring, MD
NORDA Code 440 (Ocean Rsch, Off) Bay St. Louis, MS
NRL Code 8400 (J. Walsh), Washington DC; Code 8441 (R.A. Skop), Washington DC; Rosenthal, Code 8440, Wash. DC
NSD SCE, Subic Bay, R.P.
NAVOCEANSYSCEN Hawaii Lab (D. Moore), Hawaii
NUSC Code 131 New London, CT; Code EA123 (R.S. Munn), New London CT; Code S332, B-80 (J. Wilcox)
OCEANAV Mangmt Info Div., Arlington VA
OCEANSYSLANT LT A.R. Giancola, Norfolk VA
ONR CDR Harlett, Boston MA; BROFF, CO Boston MA; Code 481, Arlington VA; Code 700F Arlington VA; Dr. A. Laufer, Pasadena CA
PMTC Pat. Counsel, Point Mugu CA
PWC CO Norfolk, VA; CO, Great Lakes IL; Code 116 (LTJG. A. Eckhart) Great Lakes, IL; Code 120C (Library) San Diego, CA; Code 128, Guam; Code 220.1, Norfolk VA; Code 30C (Boettcher) San Diego, CA
U.S. MERCHANT MARINE ACADEMY Kings Point, NY (Reprint Custodian)
US GEOLOGICAL SURVEY Off. Marine Geology, Piteleki, Reston VA
USCG (G-ECV/61) (Burkhart) Washington, DC; MMT-4, Washington DC
USCG ACADEMY LT N. Stramandi, New London CT
USCG R&D CENTER CO Groton, CT; D. Motherway, Groton CT; LTJG R. Dair, Groton CT
USNA Ocean Sys. Eng Dept (Dr. Monney) Annapolis, MD; PWD Engr. Div. (C. Bradford) Annapolis MD
AMERICAN UNIVERSITY Washington DC (M. Norton)
CALIF. DEPT OF NAVIGATION & OCEAN DEV. Sacramento, CA (G. Armstrong)
CALIF. MARITIME ACADEMY Vallejo, CA (Library)
CALIFORNIA STATE UNIVERSITY LONG BEACH, CA (CHELAPATI); LONG BEACH, CA (YEN)
CATHOLIC UNIV. Mech Engr Dept, Prof. Niedzwecki, Wash., DC
CITY OF CERRITOS Cerritos CA (J. Adams)
COLORADO STATE UNIV., FOOTHILL CAMPUS Fort Collins (Nelson)
CORNELL UNIVERSITY Ithaca NY (Serials Dept, Engr Lib.)
DAMES & MOORE LIBRARY LOS ANGELES, CA
DUKE UNIV MEDICAL CENTER B. Muga, Durham NC; DURHAM, NC (VESIC)
FLORIDA ATLANTIC UNIVERSITY BOCA RATON, FL (MC ALLISTER); Boca Raton FL (Ocean Engr Dept., C Lin)
FLORIDA ATLANTIC UNIVERSITY Boca Raton FL (W. Tessin)
FLORIDA TECHNOLOGICAL UNIVERSITY ORLANDO, FL (HARTMAN)
GEORGIA INSTITUTE OF TECHNOLOGY Atlanta GA (B. Mazanti)
INSTITUTE OF MARINE SCIENCES Morehead City NC (Director)
IOWA STATE UNIVERSITY Ames IA (CE Dept, Handy)

VIRGINIA INST. OF MARINE SCI. Gloucester Point VA (Library)
KEENE STATE COLLEGE Keene NH (Cunningham)
LEHIGH UNIVERSITY BETHLEHEM, PA (MARINE GEOTECHNICAL LAB., RICHARDS); Bethlehem PA (Fritz Engr. Lab No. 13, Beedle); Bethlehem PA (Linderman Lib. No.30, Fleckseiner)
LIBRARY OF CONGRESS WASHINGTON, DC (SCIENCES & TECH DIV)
MAINE MARITIME ACADEMY (Wyman) Castine ME; CASTINE, ME (LIBRARY)
MICHIGAN TECHNOLOGICAL UNIVERSITY Houghton, MI (Haas)
MIT Cambridge MA; Cambridge MA (Rm 10-500, Tech. Reports, Engr. Lib.); Cambridge MA (Whitman)
NATL ACADEMY OF ENG. ALEXANDRIA, VA (SEARLE, JR.)
OREGON STATE UNIVERSITY (CE Dept Grace) Corvallis, OR; CORVALLIS, OR (CE DEPT, BELL); Corvalis OR (School of Oceanography)
PENNSYLVANIA STATE UNIVERSITY State College PA (Applied Rsch Lab); UNIVERSITY PARK, PA (GOTOLSKI)
PURDUE UNIVERSITY Lafayette IN (Leonards); Lafayette, IN (Altschaeffl); Lafayette, IN (CE Engr. Lib)
SCRIPPS INSTITUTE OF OCEANOGRAPHY LA JOLLA, CA (ADAMS)
SOUTHWEST RSCH INST J. Maison, San Antonio TX; R. DeHart, San Antonio TX
STANFORD UNIVERSITY Engr Lib, Stanford CA; STANFORD, CA (DOUGLAS)
STATE UNIV. OF NEW YORK Fort Schuyler, NY (Longobardi)
TEXAS A&M UNIVERSITY COLLEGE STATION, TX (CE DEPT); College Station TX (CE Dept. Herbich)
UNIVERSITY OF CALIFORNIA BERKELEY, CA (CE DEPT, GERWICK); BERKELEY, CA (CE DEPT, MITCHELL); BERKELEY, CA (OFF. BUS. AND FINANCE, SAUNDERS); Berkeley CA (Dept of Naval Arch.); Berkeley CA (E. Pearson); La Jolla CA (Acq. Dept, Lib. C-075A); Los Angeles CA (Engr I. K. Lee); M. Duncan, Berkeley CA; SAN DIEGO, CA, LA JOLLA, CA (SEROCKI)
UNIVERSITY OF CONNECTICUT Groton CT (Inst. Marine Sci, Library)
UNIVERSITY OF DELAWARE LEWES, DE (DIR. OF MARINE OPERATIONS, INDERBITZEN); Newark, DE (Dept of Civil Engineering, Chesson)
UNIVERSITY OF HAWAII HONOLULU, HI (SCIENCE AND TECH. DIV.)
UNIVERSITY OF ILLINOIS Metz Ref Rm, Urbana IL; URBANA, IL (DAVISSON); URBANA, IL (LIBRARY); URBANA, IL (NEWARK)
UNIVERSITY OF MASSACHUSETTS (Heronemus), Amherst MA CE Dept
UNIVERSITY OF MICHIGAN Ann Arbor MI (Richart)
UNIVERSITY OF NEBRASKA-LINCOLN Lincoln, NE (Ross Ice Shelf Proj.)
UNIVERSITY OF SO. CALIFORNIA Univ So. Calif
UNIVERSITY OF TEXAS Inst. Marine Sci (Library), Port Arkansas TX
UNIVERSITY OF TEXAS AT AUSTIN Austin TX (R. Olson)
UNIVERSITY OF WASHINGTON Seattle WA (M. Sherif); SEATTLE, WA (APPLIED PHYSICS LAB); Seattle WA (E. Linger); Seattle, WA Transportation, Construction & Geom. Div
VENTURA COUNTY ENVIRON RESOURCE AGENCY Ventura, CA (Melvin)
ALFRED A. YEE & ASSOC. Honolulu HI
AMETEK Offshore Res. & Engr Div
ATLANTIC RICHFIELD CO. DALLAS, TX (SMITH)
AUSTRALIA Dept. PW (A. Hicks), Melbourne
BECHTEL CORP. SAN FRANCISCO, CA (PHELPS)
BELGIUM HAECON, N.V., Gent
BETHLEHEM STEEL CO. BETHLEHEM, PA (STEELE)
BRANDINDUS SERV INC. J. Buehler, Hacienda Heights CA
BROWN & ROOT Houston TX (D. Ward)
CANADA Can-Dive Services (English) North Vancouver; Library, Calgary, Alberta; Lockheed Petro. Serv. Ltd. New Westminster B.C.; Lockheed Petrol. Srv. Ltd., New Westminster BC; Mem Univ Newfoundland (Chari), St Johns; Surveyor, Nenninger & Chenevert Inc., Montreal; Warnock Hersey Prof. Srv Ltd, La Sale, Quebec
CHEVRON OIL FIELD RESEARCH CO. LA HABRA, CA (BROOKS)
COLUMBIA GULF TRANSMISSION CO. HOUSTON, TX (ENG. LIB.)
CONCRETE TECHNOLOGY CORP. TACOMA, WA (ANDERSON)
DRAVO CORP Pittsburgh PA (Giannino); Pittsburgh PA (Wright)
FRANCE Dr. Dutertre, Boulogne; L. Pliskin, Paris; P. Jensen, Boulogne; Roger LaCroix, Paris
GEOTECHNICAL ENGINEERS INC. Winchester, MA (Paulding)
GLOBAL MARINE DEVELOPMENT NEWPORT BEACH, CA (HOLLETT)
HALEY & ALDRICH, INC. Cambridge MA (Aldrich, Jr.)

ITALY Sergio Tattoni Milano
MAKAI OCEAN ENGRNG INC. Kailua, HI
LAMONT-DOHERTY GEOLOGICAL OBSERV. Palisades NY (McCoy); Palisades NY (Selwyn)
LIN OFFSHORE ENGRG P. Chow, San Francisco CA
LOCKHEED MISSILES & SPACE CO. INC. Sunnyvale, CA (Phillips)
LOCKHEED OCEAN LABORATORY San Diego CA (F. Simpson)
MARATHON OIL CO Houston TX (C. Seay)
MARINE CONCRETE STRUCTURES INC. MEFAIRIE, LA (INGRAHAM)
MC CLELLAND ENGINEERS INC Houston TX (B. McClelland)
MEDALL & ASSOC. INC. J.T. GAFFEY II SANTA ANA, CA
MEXICO R. Cardenas
MOBIL PIPE LINE CO. DALLAS, TX MGR OF ENGR (NOACK)
NORWAY A. Torum, Trondheim; DET NORSKE VERITAS (Roren) Oslo; I. Foss, Oslo; J. Creed, Ski; Norwegian Tech Univ (Brandtzaeg), Trondheim
OCEAN ENGINEERS SAUSALITO, CA (RYNECKI)
OCEAN RESOURCE ENG. INC. HOUSTON, TX (ANDERSON)
OFFSHORE DEVELOPMENT ENG. INC. BERKELEY, CA
PACIFIC MARINE TECHNOLOGY LONG BEACH, CA (WAGNER)
PORTLAND CEMENT ASSOC. SKOKIE, IL (COREL Y); Skokie IL (Rsch & Dev Lab, Lib.)
PRESCON CORP TOWSON, MD (KELLER)
RAYMOND INTERNATIONAL INC. E Colle Soil Tech Dept, Pennsauken, NJ
SANDIA LABORATORIES Library Div., Livermore CA
SCHUPACK ASSOC SO. NORWALK, CT (SCHUPACK)
SEATECH CORP. MIAMI, FL (PERONI)
SHELL DEVELOPMENT CO. Houston TX (C. Sellars Jr.); Houston TX (E. Doyle)
SHELL OIL CO. HOUSTON, TX (MARSHALL); Houston TX (R. de Castongrene); I. Boaz, Houston TX
SWEDEN GeoTech Inst; VBB (Library), Stockholm
TIDEWATER CONSTR. CO Norfolk VA (Fowler)
UNITED KINGDOM British Embassy (Info. Offr), Washington DC; Cement & Concrete Assoc (G. Somerville) Wexham Springs, Slou; D. New, G. Maunsell & Partners, London; Shaw & Hatton (F. Hansen), London; Taylor, Woodrow Constr (014P), Southall, Middlesex; Taylor, Woodrow Constr (Stubbs), Southall, Middlesex
WESTINGHOUSE ELECTRIC CORP. Annapolis MD (Oceanic Div Lib, Bryan)
WM CLAPP LABS - BATTELLE DUXBURY, MA (LIBRARY); Duxbury, MA (Richards)
WOODWARD-CLYDE CONSULTANTS (A. Harrigan) San Francisco; PLYMOUTH MEETING PA (CROSS, III)
AL SMOOTS Los Angeles, CA
BARA, JOHN P. Lakewood, CO
BULLOCK La Canada
F. HEUZE Boulder CO
R.F. BESIER Old Saybrook CT
WM TALBOT Orange CA